Agricultural and Forest Meteorology 376 (2026) 110895

Contents lists available at ScienceDirect

Agricultural and Forest Meteorology

journal homepage: www.elsevier.com/locate/agrformet

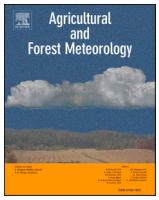

Long-term carbon sequestration and heatwave resilience in an old hemiboreal upland coniferous forest

Svyatoslav Rogozin [a,*], Alisa Krasnova [a,b], Ülo Mander [a], Veiko Uri [c], Kaido Soosaar [a]

[a] Institute of Ecology & Earth Sciences, University of Tartu, Tartu, Estonia
[b] Swedish University of Agricultural Sciences, Umeå, Sweden
[c] Institute of Forestry and Rural Engineering, Estonian University of Life Sciences, Tartu, Estonia

ARTICLE INFO

Keywords:
Carbon dioxide
Eddy covariance
Heatwave
Hemiboreal forest
Interannual variability
Net ecosystem production

ABSTRACT

Boreal forests play an important role in the global carbon cycle due to their extensive area and ability to sequester a considerable amount of atmospheric carbon dioxide (CO_2). They are generally stable ecosystems that function as carbon sinks. However, their sink capacity is vulnerable to the impact of extreme weather conditions. In this study, we aim to investigate the multi-year and seasonal carbon dynamics of an old upland coniferous forest in the hemiboreal zone, identify the main environmental drivers influencing annual NEP, and explore the potential legacy effects of the 2018 heatwave. Over an eight-year period (2016–2023), the forest shifted from a carbon sink (mean net ecosystem productivity (NEP) of 238 ± 52 g C m^{-2} $year^{-1}$) to a carbon-neutral state in 2020 (NEP = -2 ± 5 g C m^{-2} $year^{-1}$) and back to a net carbon sink (NEP = 136 ± 50 g C m^{-2} $year^{-1}$). The average NEP over the eight-year period was 170 ± 42 g C m^{-2} $year^{-1}$. Our research showed no significant year-to-year changes in GEP during the study period, while the changes in R_{eco} were substantial. Our results confirm that air temperature has the greatest influence on annual NEP. The warmest autumn over the past 19 years, recorded in 2020, and an atypical June together resulted in a noticeable increase in ecosystem respiration, which shifted annual NEP towards negative net values, while no significant impact on GEP was found. Additionally, our study found that the old upland hemiboreal forest showed no legacy effect in the years following the 2018 heatwave, demonstrating its resilience to extreme temperature events. Our results underscore the importance of continuous monitoring carbon dynamics variability to determine the ecosystem's resilience to seasonal temperature fluctuations and to inform management strategies for forests preservation.

1. Introduction

The forested regions on Earth measure 4.06 billion hectares (ha), equating to 31 % of the planet's land area (FAO, 2020). Boreal forests cover a significant portion, approximately 27–30 %, of the world's forested areas, estimated as the second largest forest domain globally, following the tropical forest domain (Baldocchi et al., 2000; Potapov et al., 2008; FAO, 2020). They serve as a significant sink of atmospheric carbon dioxide (CO_2) due to their vast expanse and capacity for substantial carbon storage (Bonan, 2008; Dixon et al., 1994). Hemiboreal forests, located at the southern border of the boreal zone, represent a transitional zone characterized by higher variability in species richness and environmental conditions (Ahti et al., 1968; Hytteborn et al., 2005; Jõgiste et al., 2018). This unique position makes these forests potentially more vulnerable to extreme weather events (Froelich et al., 2015). Considering the probability of the zone shifting further north in the future due to changing climatic conditions (Hickler et al., 2012), it is crucial to conduct research of carbon dynamics in these areas (Krasnova et al., 2019, 2022). Northern coniferous forests are typically stable ecosystems that function as significant net carbon sinks (Chan et al., 2018; Ilvesniemi et al., 2009; Launiainen et al., 2022; Suni et al., 2003). However, under the influence of various factors, they can sometimes shift from being carbon sinks to net carbon sources (Froelich et al., 2015; Hadden and Grelle, 2016a; Ueyama et al., 2014). Previous studies have demonstrated that forest carbon dynamics is influenced by various meteorological factors, including air and soil temperatures (Barr et al., 2009; Barr et al., 2007; Bergeron et al., 2007; Chen et al., 2006), moisture availability (Dunn et al., 2007; Krishnan et al., 2008) and solar radiation (Barr et al., 2009; Krishnan et al., 2008). Furthermore, periodic disturbances such as fire (Mkhabela et al., 2009), insects (Stephens

* Corresponding author at: Vanemuise 46, Tartu 51003, Estonia.
E-mail address: svyatoslav.rogozin@ut.ee (S. Rogozin).

https://doi.org/10.1016/j.agrformet.2025.110895
Received 6 September 2024; Received in revised form 31 July 2025; Accepted 15 October 2025
Available online 25 October 2025

et al., 2018), harvesting (Kurz et al., 2008; Kurz and Apps, 1999) and extreme weather events such as storms (Lindroth et al., 2009) and heatwaves (Ciais et al., 2005; Krasnova et al., 2022; Lindroth et al., 2020; Mamkin et al., 2022) also noticeably influence forest carbon dynamics. There have been very few long-term studies focused on the carbon dynamics and heatwave legacy effect in hemiboreal forests. In the context of global warming, the response of hemiboreal forests' carbon dynamics to heatwaves becomes particularly intriguing, since their frequency and duration are predicted to increase (Barriopedro et al., 2011; Perkins and Alexander, 2013; Perkins and Lewis, 2020). In the summer of 2018, Estonia, along with Western Europe and Scandinavia, experienced a heatwave comparable to the same extreme weather events in 2003 and 2010 (Bastos et al., 2020). Although heatwave impacts on boreal and temperate forests have received some attention, studies addressing legacy effects remain limited, particularly in hemiboreal ecosystems. The legacy effect could be defined as the prolonged influence of extreme events on forest functioning that persists beyond the immediate disturbance period and potentially affects carbon uptake, productivity or phenology in subsequent seasons (Anderegg et al., 2015). In the study by Krasnova et al. (2022), it was found that the heatwave had a varying impact on hemiboreal forests; however, the authors limited their comparison to 2017 and 2018 and did not investigate the legacy effect. Earlier findings regarding the legacy effect have shown that forests composed of both coniferous and broadleaved trees demonstrated greater resilience to the drought stress caused by the 2003 heatwave compared to monoculture forests (Pretzsch et al., 2013). Additionally, it has been found that coniferous forests were less sensitive to drought than broadleaf forests (De Boeck et al., 2010; Granier et al., 2007). Afterwards, (Matkala et al., 2021) confirmed that pine forests have a higher resilience to warm and dry conditions than spruce forests. Since Estonia's forests are predominantly evergreen coniferous forests, with pine, spruce, and birch as the dominant species (Republic of Estonia environmental agency, 2021), these findings underscore the need to study the heatwave legacy effect in countries like Estonia, which lies on the southern edge of the boreal zone and may therefore experience amplified impacts. To assess the carbon dynamics and heatwave legacy effect in the old upland hemiboreal forest, we used data from eight years (2016–2023) of CO_2 flux (net ecosystem exchange) measured with the eddy covariance (EC) system. The aims of this study were: 1) To investigate the multi-year dynamics of upland hemiboreal forest carbon exchange, 2) To study seasonal dynamics and the main environmental drivers that influence annual NEP, and 3) To explore the presence of heatwave legacy effect and enhance our understanding of how the coniferous hemiboreal forest might respond to extreme events in the future.

2. Materials and methods

2.1. Site description

The data for this study were collected at the Soontaga forest station (Fig. 1), established in South-Estonia (58°01′24.802″N, 26°04′14.98″E). The climate of Estonia is characterized as hemiboreal with the influence of the Baltic Sea, resulting in harsh winters and warm summers. Southern Estonia has milder winter conditions compared to northern regions, with a more stable snow cover. The summer period in the southern part of the country is marked by higher temperatures and increased sunshine hours, leading to warmer and longer days.

The Soontaga tower is located in an overmature (average 220-year-old) coniferous forest stand (Fig. 2), with the first layer dominated by Scots pine (*Pinus sylvestris* L.), while the secondary layer is comprised of Norway spruce (*Picea abies* L. *Karst*).

The total station footprint area is 21.4 hectares. The footprint covers 26 forest stands at different development stages. In our study, we grouped the forest stands by age categories (Table 1): 60–70 years as middle-aged forests, 70–100 years as premature forests, 100–150 years

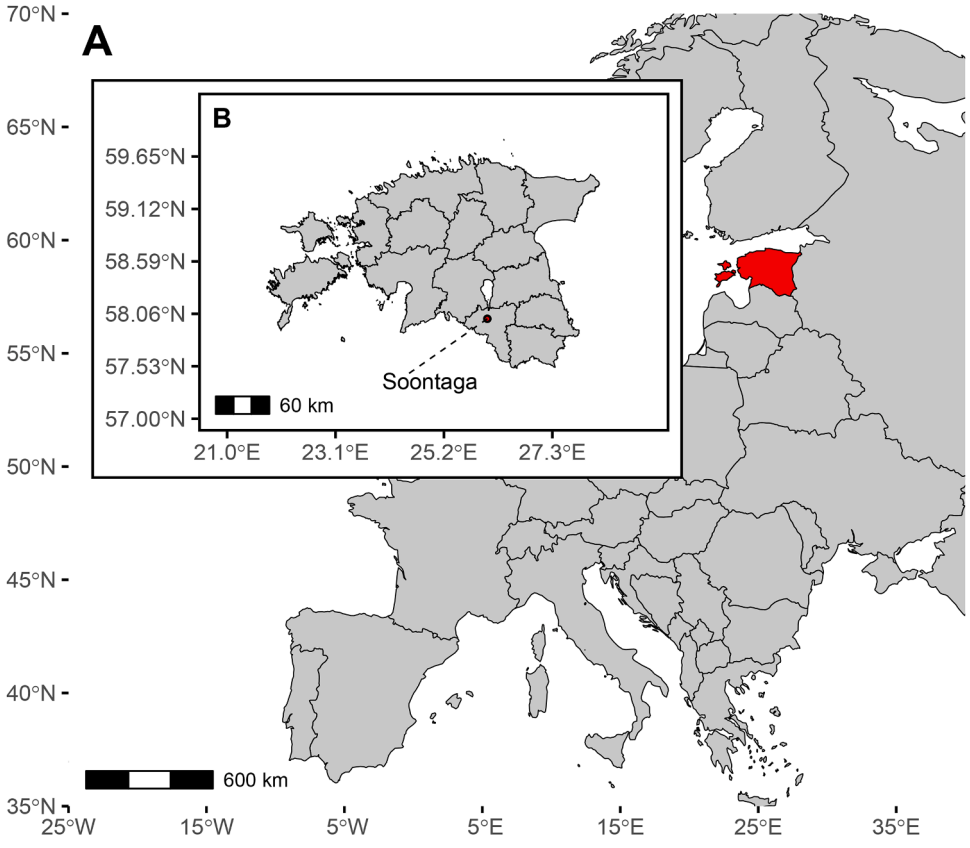

Fig. 1. (A) Location of Estonia in Europe, (B) Location of Soontaga station in Estonia.

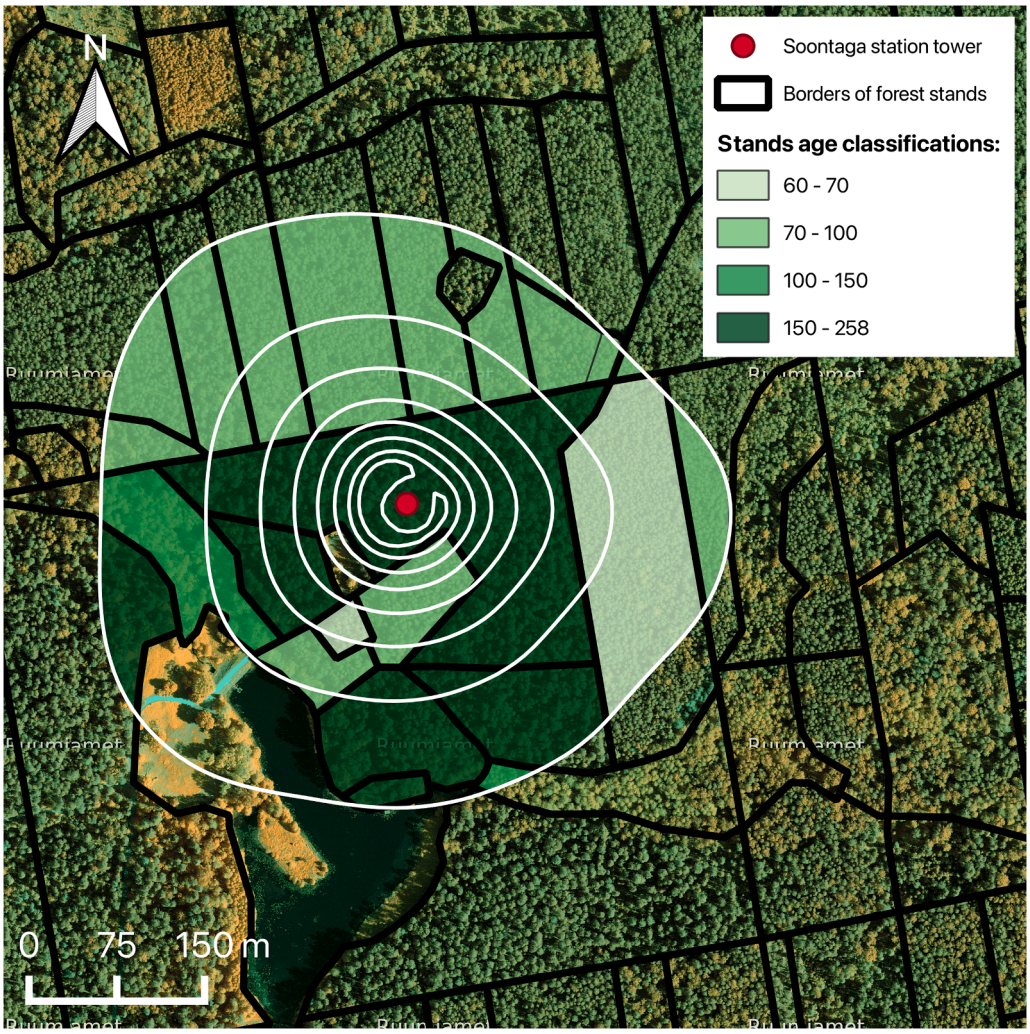

Fig. 2. Soontaga tower footprint area (model by Kljun et al. (2015)). The red point indicates the location of Soontaga tower, the white lines represent the aggregated footprint borders (ranging from 10 % to 80 %), and the black lines outline the borders of the forest stands. The green areas, ranging from light green (youngest) to dark green (oldest), represent forest stands of different age groups within the 80 % footprint. The age classifications are indicated in years.

Table 1
Soontaga 80 % of footprint area distribution by age group. NA group indicates that no information about the area (part of the lake and forestless area) is available.

Age group (years old)	Area (hectares)	Percentage of 80 % footprint
NA	2.0	9.6 %
60–70	2.4	11.3 %
70–100	7.8	36.3 %
100–150	1.1	5.2 %
150 +	8.0	37.5 %

as mature forests, and 150+ years as overmature forests (Fig. 2). On the southwest border of the footprint, there is a section of a lake. Near the station, also to the southwest, there is a forestless area. To the northeast of the footprint, there is a clear-cut area made in 2022 (Fig. 2 shows orthophotos from 2021).

Across all stands, the first layer is primarily composed of Scots pine, while the secondary layer features Norway spruce. All stands belonged to the *Rhodococcum* or *Oxalis-Rhodococcum* site type, according to local classification (Lõhmus, 1984). The soil type is *Endogleyic Albic Podzol (Arenic)*. The site is characterized by its dry conditions and a low water table.

In our study, we named the Soontaga forest as an "old forest" based on two key factors. First, our calculations of the maximum relative contribution show that at a distance of 29.8 m from the tower, where the vegetation has the greatest impact on the signal, only overmature forest stands are present. Second, within the 60 % footprint boarders, the majority of the area is covered by mature and overmature forest stands.

As typical for mesotrophic pine stands on sandy soils, dwarf shrubs and mosses form the main share of the biomass of the understorey plants at all studied stands of different ages. The dominating species were lingonberry (*Vaccinium vitis-idaea L*) and blueberry (*Vaccinium myrtillus L*). The dominating moss species were red-stemmed feathermoss (*Pleurozium schreberi* (Brid.) Mitt.) and glittering woodmoss (*Hylocomium splendens* (Hedw.) B., S & G.). The average biomass of ground vegetation across all stands was 6.40 ± 0.46 t ha^{-1}, estimated in 2015 according to the methodology described by Uri et al. (2019, 2022).

2.2. Instrumentation

The fluxes of CO_2 were estimated using the eddy covariance (EC) system mounted on a 39 m scaffolding tower, 7 m above the canopy. The CO_2 concentrations were measured using a LI-7200 enclosed-path gas analyser (LI-COR Biosciences, Lincoln, NE, USA) and 3D wind speed was measured by a Metek uSonic-3 Class A MP ultrasonic anemometer (METEK GmbH, Elmshorn, Germany). Both measurements were performed at a sampling frequency of 10 Hz. Global downwelling

shortwave radiation (Rg) was measured using a Kipp & Zonen CMP22 pyranometer (Kipp & Zonen, Delft, The Netherlands). In order to obtain a long-term dataset, we opted to use air temperature readings from the Tõravere weather station (58°15′51'' N, 26°27′41'' E), located 36 km from the site. Soil water content (SWC) was continuously measured with four ML3 ThetaProbe sensors (Delta-T Devices Ltd, Cambridge, United Kingdom): two sensors at 10 cm depth (SWC_{10}) and two sensors at 40 cm depth (SWC_{40}).

2.3. Flux calculation and post-processing

The eight years (2016–2023) of carbon fluxes were calculated as the covariance between CO_2 mixing ratios and vertical wind speeds utilizing the EddyPro software (version 7.0.9, LI-COR Biosciences, USA) and a standard averaging interval of 30 min. High-frequency data processing included despiking (Mauder et al., 2013), double rotation tilt correction, time lag compensation and block averaging. Spectral correction on low-frequency range was done using the Moncrieff et al. (1997) method and high-frequency correction as detailed by Moncrieff et al. (2005). Periods of technical maintenance, power outages, and other disturbances in measurements were removed from the analysis.

Net ecosystem production (NEP) was calculated as a sum of EC fluxes and flux storage. The latter was calculated using the tower-top method. Following the traditional ecological sign convention, we inverted the sign of NEP so that positive values indicate net carbon sequestration (i.e., the ecosystem acts as a carbon sink), while negative values indicate net carbon release to the atmosphere.

All physically implausible NEP values (below −100 or above 50 μmol m^{-2} s^{-1}) were filtered out. To exclude periods of low turbulence, the friction velocity (u*) thresholds were estimated for each year using the moving point test method by Papale et al. (2006) implemented in the ReddyProc R package (available at https://github.com/bgctw/REddyProc) developed by Wutzler et al. (2018). The mean u* value over an eight-year period was 0.23 m s^{-1}. We removed half-hourly NEP observations recorded when u* fell below the year-specific threshold. We chose to apply u* filtering not only to time values but to the full dataset to partially compensate for the limitations of the tower-top storage estimation method. The u* thresholds and the amount of available quality-controlled data retained after u* filtering is available in Appendix 1. After the u* filtering, left-over NEP spikes were removed from the analysis. Spikes were identified as values outside of three times the standard deviation from the mean of a 14-day moving window. To obtain monthly and annual NEP estimates, we gap-filled the dataset using the marginal distribution sampling (MDS) approach (Reichstein et al., 2005a). Gross Ecosystem Production (GEP) and Ecosystem Respiration (R_{eco}) were partitioned using the night-time method as implemented in the ReddyProc package (Wutzler et al., 2018), which builds upon the temperature-response framework described by Reichstein et al. (2005b). GEP is reported as a positive flux representing carbon uptake via photosynthesis, and R_{eco} as a positive flux representing carbon loss to the atmosphere.

In the absence of direct measurements, heterotrophic respiration (R_h) was estimated by a simplified method proposed by Litton et al. (2007) and previously used by (Lindroth et al., 2020) for various boreal and hemiboreal coniferous forest stands. First, autotrophic respiration (R_a) was calculated as a fraction of GEP (Eq. (1)), and then R_h was estimated as a difference between R_{eco} and R_a (Eq. (2)).

$$R_a = 0.57 * GEP, \tag{1}$$

where 0.57 is the coefficient offered by Litton et al. (2007) for needleleaf evergreen forests, and GEP is gross ecosystem production (g C m^{-2} $month^{-1}$).

$$R_h = R_{eco} - R_a, \tag{2}$$

where, R_{eco} is ecosystem respiration (g C m^{-2} $month^{-1}$) and R_a is autotrophic respiration (g C m^{-2} $month^{-1}$).

We acknowledge that our approach assumes a temporally invariant R_a/GEP ratio, which likely oversimplifies the complexity of respiration partitioning under changing environmental and phenological conditions. Additionally, since R_{eco} values are derived from nighttime flux measurements and extrapolated to entire days, this introduces further uncertainty into R_h estimates. Nevertheless, in the absence of direct R_h measurements at the site, we adopted this pragmatic method to ensure consistency in evaluating seasonal and interannual dynamics of R_h. It is important to emphasize that we interpret R_h variability in a relative rather than absolute sense, and our estimates are not intended for direct comparison with chamber-based measurements from other forest ecosystems.

2.4. Uncertainties

Our estimated u* thresholds varied substantially across years, ranging from 0.17 m s^{-1} in 2020 to 0.32 m s^{-1} in 2018 (Appendix 1), representing nearly a twofold difference at a single site. As shown in Appendix 1, higher u* thresholds systematically exclude a larger fraction of data, while lower thresholds retain more observations. For example, 2020, with the lowest threshold, resulted in the highest data retention. To assess whether this variability biased our long-term carbon flux estimates, we conducted a parallel analysis using a fixed u* threshold of 0.20 m s^{-1} for all years. The fixed-threshold results are presented in Appendix 2 alongside the variable-threshold analysis for direct comparison. In both approaches, the nine-year dynamics in NEP, GEP, and R_{eco} remained consistent, confirming the robustness of our interannual flux dynamics with respect to the u* threshold selection.

To quantify the annual uncertainty introduced by the MDS gap-filling procedure, we implemented an adapted bootstrap approach: the 20 % of measured half-hourly NEE in each year were randomly removed 200 times. After that, MDS gap-filling algorithm was rerun using the same corresponding annual u* threshold. The reconstructed values at the artificially omitted positions were then compared with their original measurements, yielding two primary error metrics: mean bias error (MBE) and root-mean-square error (RMSE) at the half-hourly resolution. Half-hourly RMSE and MBE values were converted to annual values (Eq. (3) and 4) and expressed in g C $year^{-1}$ (Appendix 1).

$$RMSE_{year} = \sqrt{N_{slots}} * t * M * \sqrt{\frac{1}{B}\sum_{b=1}^{B}\left(\frac{1}{n_b}\sum_{i\in rem_b}\left(y_i^{(b)} - y_i\right)^2\right)}, \tag{3}$$

$$MBE_{year} = N_{slots} * t * M * \left(\frac{1}{B}\sum_{b=1}^{B}\left(\frac{1}{n_b}\sum_{i\in rem_b}\left(y_i^{(b)} - y_i\right)\right)\right), \tag{4}$$

where N_{slots} is the number of half-hourly intervals in a year, t is the duration of each interval (1800 s), M is the conversion factor from μmol CO_2 to grams of carbon (12×10^{-6} g C per μmol CO_2), B is the total number of bootstrap replicates, n_b is the number of points removed in the b_{th} replicate, rem_b is the set of indices of those removed points, $y_i^{(b)}$ is the gap-filled value at index in the b_{th} replicate (μmol CO_2 m^{-2} s^{-1}), and y_i is the original measured value at index i (μmol CO_2 m^{-2} s^{-1}).

While RMSE remains relatively stable across years, the MBE values exhibit greater interannual variability, ranging from a slight underestimation (−1.77 g C $year^{-1}$ in 2023) to a noticeable overestimation (up to 19.70 g C $year^{-1}$ in 2017) (Appendix 1). This indicates that while random errors are well controlled, low-level bias in the gap-filling procedure can still vary depending on year-specific conditions.

The second major source of systematic uncertainty in annual NEP, GEP, and R_{eco} estimates arises from the potential underestimation of R_{eco} during calm night-time periods. To quantify this, we followed the bootstrapping approach of Wutzler et al. (2018), calculating annual NEP, GEP, and R_{eco} across a distribution of 39 u* threshold scenarios based on percentiles from 2.5 % to 97.5 %. For each flux, we then

measured the difference between the maximum and minimum values across the u* scenarios and expressed that difference as a percentage of the median value. The resulting u* uncertainties are summarized in Table 2.

Overall, data quality across years appears robust, particularly for GEP and R_{eco}, with relative errors mostly below 3 %. NEP shows moderate variability in uncertainty, which is expected due to its nature as a net flux. The exceptionally large relative uncertainty for NEP in 2020 (234.5 %) arises because the mean NEP that year was very close to zero, so even a modest absolute standard deviation corresponds to a very high percentage.

All further analysis and representations in the current study are based on gap-filled fluxes. While NEP is directly measured by the EC system, R_{eco} is partially modelled through the extrapolation of nighttime NEP-temperature relationships, and GEP, as the sum of NEP and R_{eco}, is also partially model-based. R_h, in turn, is a fully derived component based on these fluxes. As a result, the degree of model dependence increases from NEP to R_h, and this hierarchy should be taken into account when interpreting the different fluxes. In particular, R_{eco} plays a central role in flux partitioning, as it directly influences both GEP and R_h. Although we followed a widely accepted approach for estimating R_{eco}, its accuracy remains sensitive to the availability of night-time data, which is often limited due to u* filtering.

2.5. Data analysis

Since R_{eco} variability played a major role in our study, we used the random forest method to analyse the possible interannual variability of R_{eco} environmental drivers. Random forests regression models have increasingly been employed to study the carbon cycling processes (Braybrook et al., 2021; López-Blanco et al., 2017; H. Zhang et al., 2017) due to their superior predictive capabilities and as a non-parametric methodology for assessing the significance of variables (Breiman, 2001). In this study, a random forest machine-learning regression algorithm was performed using caret (Kuhn, 2008) and mlbench (Leisch and Dimitriadou, 2021) packages in R version 4.3.2 (R Core Team, 2021). The algorithm was applied to daily averages of measured R_{eco} to estimate the absolute importance of meteorological variables on an annual scale. To increase the accuracy of the results, we ran each year 10 times and took the mean absolute importance for each meteorological variable. In each model run, the data were split into a training set (50 %) and a validation set (50 %). The variables included to model daily ecosystem respiration were air temperature, SWC_{10}, SWC_{40} and precipitation. The R^2, RMSE, and MAE values for the random forest models are in Appendix 3. The 2023 data was not included in this analysis due to a lack of sufficient good-quality SWC data.

To compare autumn (September, October, November) R_{eco} temperature response and temperature sensitivity (Q_{10}) in different years, median daily values of air temperature and night-time respiration were used with the Q_{10} model (Barba et al., 2018; Hoff and Lehfeldt, 1899) (Eq. (5)). Models with a coefficient of determination (R^2) below 0.3 were considered insufficiently predictive and excluded from further analysis.

$$R_{eco} = F_{10} * Q_{10}^{\left(\frac{T-10}{10}\right)}, \quad (5)$$

where R_{eco} is the night-time measured respiration (μmol m^{-2} s^{-1}), F_{10} is the flux at 10 °C (μmol C m^{-2} s^{-1}), Q_{10} is temperature sensitivity of the flux (unitless), and T is measured air temperature (°C).

To quantify the relationship between GEP and solar radiation and calculate photosynthetic capacity (GEP_{max}), we utilized a modified version of the Michaelis-Menten light response curve model (Eq. (6)).

$$GEP = \frac{\alpha * Rg * GEP_{max}}{\alpha * Rg + GEP_{max}}, \quad (6)$$

where α is light use efficiency (μmol C J^{-1}), Rg is global radiation (W m^2), GEP is gross ecosystem production (μmol m^{-2} s^{-1}), and GEP_{max} is the maximum photosynthetic capacity that represents the maximum possible amount of carbon that the forest can absorb over a specific period (μmol m^{-2} s^{-1}). Estimated residuals were tested for significance ($p < 0.05$). Models with R^2 below 0.3 were considered insufficiently predictive and excluded from analysis.

To estimate the significance of carbon fluxes and environmental variables differences on inter-annual scale, we used the Wilcoxon signed-rank test on daily means. To identify months with the most pronounced anomalies in carbon fluxes or environmental conditions, we applied an interquartile range (IQR)-based outlier detection approach. For each variable, monthly distributions were evaluated across the entire observation period. Within each calendar month, the first (Q_1) and third (Q_3) quartiles were calculated, and the IQR was defined as the difference between them. A month was classified as anomalous if the observed value fell below Q_1 – 1.5 * IQR or exceeded Q_3 + 1.5 * IQR, indicating a moderate statistical outlier.

All data analyses were performed using the R environment (R version 4.3.2, http://www.r-project.org).

3. Results

3.1. Inter-annual variability of environmental parameters and carbon fluxes

The inter-annual temperature pattern varied, with 2020 being warmer than the long-term mean by 1.2 °C (Fig. 3A). In contrast, 2017 and 2021 were relatively cold years, with mean temperatures 0.9 °C and 0.7 °C below the long-term average, respectively. The annual vapour pressure deficit (VPD) notably deviated from the long-term average only in the years 2016 (+39.1 %) and 2017 (−30.9 %) (Fig. 3B). In the remaining years, there were no significant differences ($p > 0.05$) from the multi-year average. Annual global radiation was stable over the studied period, with a slightly higher amount in 2016 (+7.8 %) and lower in 2017 (−7.2 %). (Fig. 3C). The year 2016 received the highest amount of precipitation (22.6 % above average), while 2018 and 2022 received significantly less (−17.0 % and −24.3 %, respectively) (Fig. 3D). Annual SWC was the highest in 2016, followed by a decrease and reaching the minimum in 2018 (10.3 % lower than long-term average) with a subsequent increase over the 2019–2022 (Fig. 3E-F). We did not find any statistically significant trends in annual environmental factors over the studied eight years.

During the study, the ecosystem switched from acting as a net carbon sink to a carbon-neutral forest in 2020 and back (Fig. 4). NEP varied from a maximum of 309 ± 14 g C m^{-2} $year^{-1}$ in 2016 to a minimum of -2 ± 5 g C m^{-2} $year^{-1}$ in 2020, with an overall average of 170 ± 42 g C m^{-2} $year^{-1}$. The yearly changes in GEP varied from a maximum value of 1357

Table 2
Relative uncertainties (g C m^{-2} $year^{-1}$) in annual NEP (net ecosystem production), R_{eco} (ecosystem respiration), and GEP (gross ecosystem production) estimates calculated as the range across u* scenarios, expressed as a percentage of the median. Percentages in parentheses indicate how large the uncertainty range is relative to the annual flux.

Year	NEP relative uncertainty (g C m^{-2} $year^{-1}$) (%)	R_{eco} relative uncertainty (g C m^{-2} $year^{-1}$) (%)	GEP relative uncertainty (g C m^{-2} $year^{-1}$) (%)
2016	14 (4.5 %)	26 (2.5 %)	16 (1.2 %)
2017	4 (1.4 %)	20 (2.0 %)	14 (1.1 %)
2018	10 (3.7 %)	34 (3.6 %)	24 (2.0 %)
2019	6 (7.2 %)	35 (3.0 %)	28 (2.2 %)
2020	5 (234.5 %)	40 (3.1 %)	33 (2.6 %)
2021	3 (6.1 %)	18 (1.5 %)	14 (1.1 %)
2022	6 (4.4 %)	22 (2.1 %)	22 (1.8 %)
2023	8 (3.6 %)	22 (2.0 %)	16 (1.2 %)

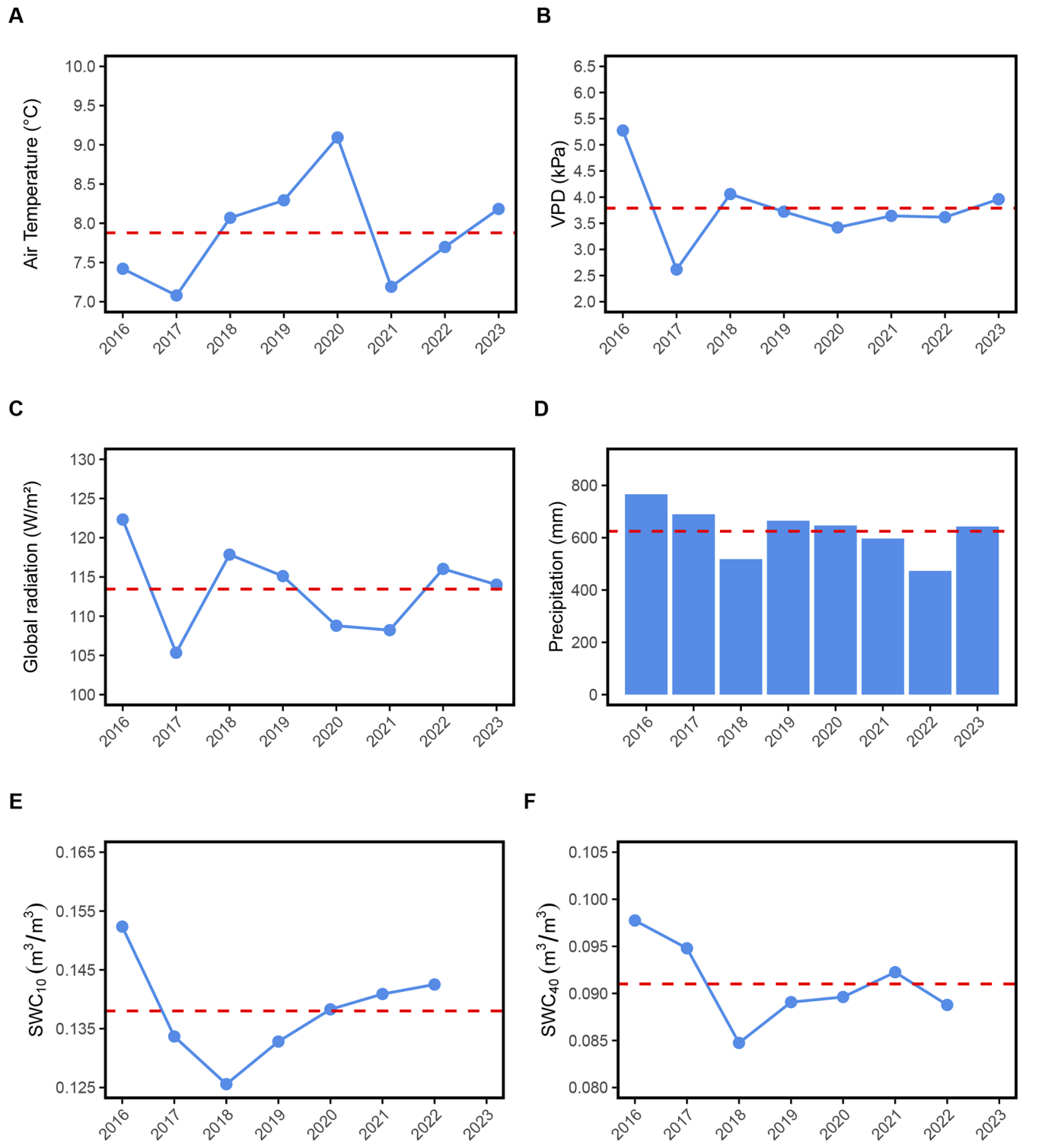

Fig. 3. Inter-annual variability of meteorological variables: average air temperature (A), average vapor pressure deficit (VPD, B), average global radiation (C), sums of precipitation (D), average soil water content at 10 cm depth (SWC_{10}, E), average soil water content at 40 cm depth (SWC_{40}, F). The red dashed line represents the eight-year mean value for each variable.

$\pm$ 16 g C m^{-2} $year^{-1}$ in 2016 down to 1198 $\pm$ 22 g C m^{-2} $year^{-1}$ in 2022, averaging 1273 $\pm$ 53 g C m^{-2} $year^{-1}$. Meanwhile, R_{eco} showed annual fluctuations from 1293 $\pm$ 40 g C m^{-2} $year^{-1}$ in 2020 to 946 $\pm$ 34 g C m^{-2} $year^{-1}$ in 2018, with a mean value of 1103 $\pm$ 111 g C m^{-2} $year^{-1}$.

A Wilcoxon signed-rank test demonstrated that daily NEP and R_{eco} in the years 2019, 2020, and 2021 were statistically distinct from all other years ($p < 0.05$). In contrast, daily GEP values did not show any statistical difference over these three years, suggesting that photosynthetic activity does not show notable statistical variation during this timeframe.

3.2. Seasonal variability of environmental parameters and carbon fluxes

Air temperature pattern is distinctive for the Northern Hemisphere,

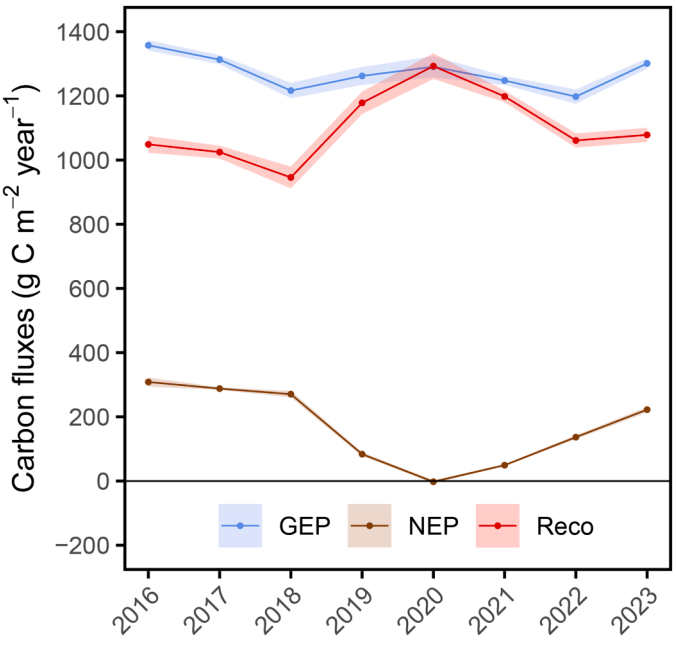

Fig. 4. Interannual variability of carbon fluxes: gross ecosystem production (GEP), net ecosystem production (NEP), and ecosystem respiration R_{eco}. The shaded area represents uncertainty.

with the rise in February, reaching a peak in June and July, then a gradual decrease towards December (Fig. 5A). It is worth noting that high temperatures in October and November 2020 (9.8 ± 3.7 °C and 5.0 ± 3.0 °C, respectively), made them the warmest for the last 18 years (Appendix 4). Additionally, June and July of 2021 stood out with high average temperatures of 20.8 ± 3.5 °C and 22.6 ± 3.2 °C, making them the warmest months of the last ten years (Appendix 4). All these deviations were identified as outliers based on the IQR criterion. Notably, March 2018 and November 2016 were identified as cold anomalies, with mean temperatures 3.9 °C and 2.8 °C lower than the respective long-term monthly averages, while May 2018 stood out as a warm anomaly, exceeding the monthly mean by 4.6 °C.

Between 16 July and 3 August 2018, the heatwave was observed in the Soontaga area (Krasnova et al., 2022). Although the monthly mean temperature for July 2018 ranked only second highest in the 2016–2023 period, the most extreme daily temperatures occurred at the transition from July to August. Averaging over the entire month obscures this effect. For clarity, Appendix 7 presents the mean values and standard deviations of daily air temperature for the period 15 July–5 August of each year. The highest mean temperature was recorded in 2018 at 24.2 ± 1.6 °C, followed by 2021 (20.1 ± 3.2 °C) and 2016 (19.5 ± 2.0 °C). The lowest average was observed in 2017 (17.6 ± 1.7 °C). This analysis confirms the presence of anomalously high air temperatures, which substantiates the occurrence of a heatwave in the specified interval.

From 2016 to 2023, the dynamics of VPD showed notable variations across different months and seasons (Fig. 5B). The highest VPD was recorded in July 2016 at 19.1 hPa, 117.6 % above the eight-year July mean of 8.8 ± 4.6 hPa. In spring, anomalies were most pronounced in March 2022 at 2.8 hPa, 55.2 % above the March mean of 1.8 ± 0.6 hPa, and in April 2019 at 7.3 hPa, 72.1 % above the April mean of 4.2 ± 1.5 hPa. In autumn, October 2021 climbed to 2.4 hPa, 51.6 % above the October mean.

Rg dynamics (Fig. 5C) show a consistent year-to-year pattern, with a nearly identical curve shape indicating the repeatability of seasonal changes in solar radiation. This pattern, typical for the northern hemisphere, demonstrates higher radiation levels during May and the summer months (June, July, and August), gradually decreasing towards the winter months. Rg varied from the overall highest, 283.3 W/m^2 in May 2018, to the overall lowest, 5.7 W/m^2 in December 2018. Despite identical curve patterns, some fluctuations can be observed, suggesting minor annual variations in the intensity of solar radiation. In spring, the most pronounced anomalies occurred in March 2022, when Rg reached 121.0 W/m^2, 30.2 % above the March mean of 92.9 ± 14.0 W/m^2, and in April 2019 at 196.7 W/m^2, 24.1 % above the April mean of 158.5 ± 18.4 W/m^2. During summer, the highest value was recorded in July 2021 at 254.1 W/m^2, 16.7 % above the eight-year July mean of 217.8 ± 17.2 W/m^2. In autumn, October 2021 still stood out with 57.5 W/m^2, which is 24.8 % above the October average of 46.0 ± 5.8 W/m^2.

From Fig. 5D, it is clearly visible that the level of precipitation does not follow the strict seasonal pattern as global radiation. In contrast to the consistent rise and fall of radiation levels with the coming of summer and winter, the amount of precipitation shows significant variability both within a single year and when comparing different years. Sharp spikes in some months are indicative of periods with more intense rainfall. For example, in June 2016, 204.8 mm of precipitation fell, which is 2.5 times more than the eight-year average for June. The driest month was May of the same year, when only 1.9 mm of precipitation was recorded.

The overall dynamics of SWC (Figs. 5E and 5F) at depths of 10 and 40 cm reflect a distinct seasonal pattern that repeats from year to year. February, March, and April are characterized by an increase in soil water content. In mid to late May, as well as during the summer months (June, July, August), soil moisture significantly decreases. In the autumn (September, October, November) and December, there is a slight increase in moisture content. During this study, the month with the least amount of water at a depth of 10 cm was August, with an average of 0.12 ± 0.02 m^3/m^{-3}, while the most was in March at 0.16 ± 0.02 m^3/m^{-3}. At a depth of 40 cm, the least amount of water was in May at 0.08 ± 0.01 m^3/m^{-3}, and the most was in March at 0.1 ± 0.01 m^3/m^{-3}. Additionally, a period from February to August 2016 is notable, when unusually high values of SWC were recorded at both depths.

We did not find any statistically significant trends ($p < 0.05$) in monthly and seasonal environmental factors.

Since the annual net balance is a result of monthly variation, we investigated the seasonal variability of carbon exchange components. NEP, GEP and R_{eco} and R_h peak during the summer months when conditions are most optimal for photosynthesis and respiration and significantly decline during the winter months (Fig. 6).

We identified months with the most outstanding deviations in carbon fluxes relative to the eight-year monthly means using an interquartile-range (IQR)–based outlier detection criterion. These statistically significant months are summarized in Table 3. Several of these months cluster into periods that correspond to elevated annual R_{eco}. For example, R_{eco} in June 2020 alone was 15.7 % of the annual R_{eco}, while the October and November of 2020 together were 13.1 % of the total annual R_{eco}. Furthermore, the combined R_{eco} for June and July of 2021 was 41 % of the annual R_{eco}.

3.3. *Environmental drivers of ecosystem respiration*

NEP is a net result of the two opposite fluxes, GEP and R_{eco}. However, we decided to focus on exploring R_{eco} drivers because of significant ($p < 0.05$) changes in annual R_{eco}, while interannual variation in GEP was not significant ($p > 0.05$). Data analysis conducted using the random forests method shows that the ensemble and importance of R_{eco} environmental drivers were similar over the seven years of observations, with air temperature being consistently the most important predictor (Fig. 7).

The SWC at a depth of 10 cm consistently held second place in significance, indicating that the moisture of the upper soil layer plays an important role in the ecosystem respiration process. At the same time, SWC at a depth of 40 cm took third place, underscoring a lesser but still noticeable impact of deep moisture on respiratory processes. The amount of precipitation, although remaining the least important of the factors considered, still showed a significant increase in its role in 2019

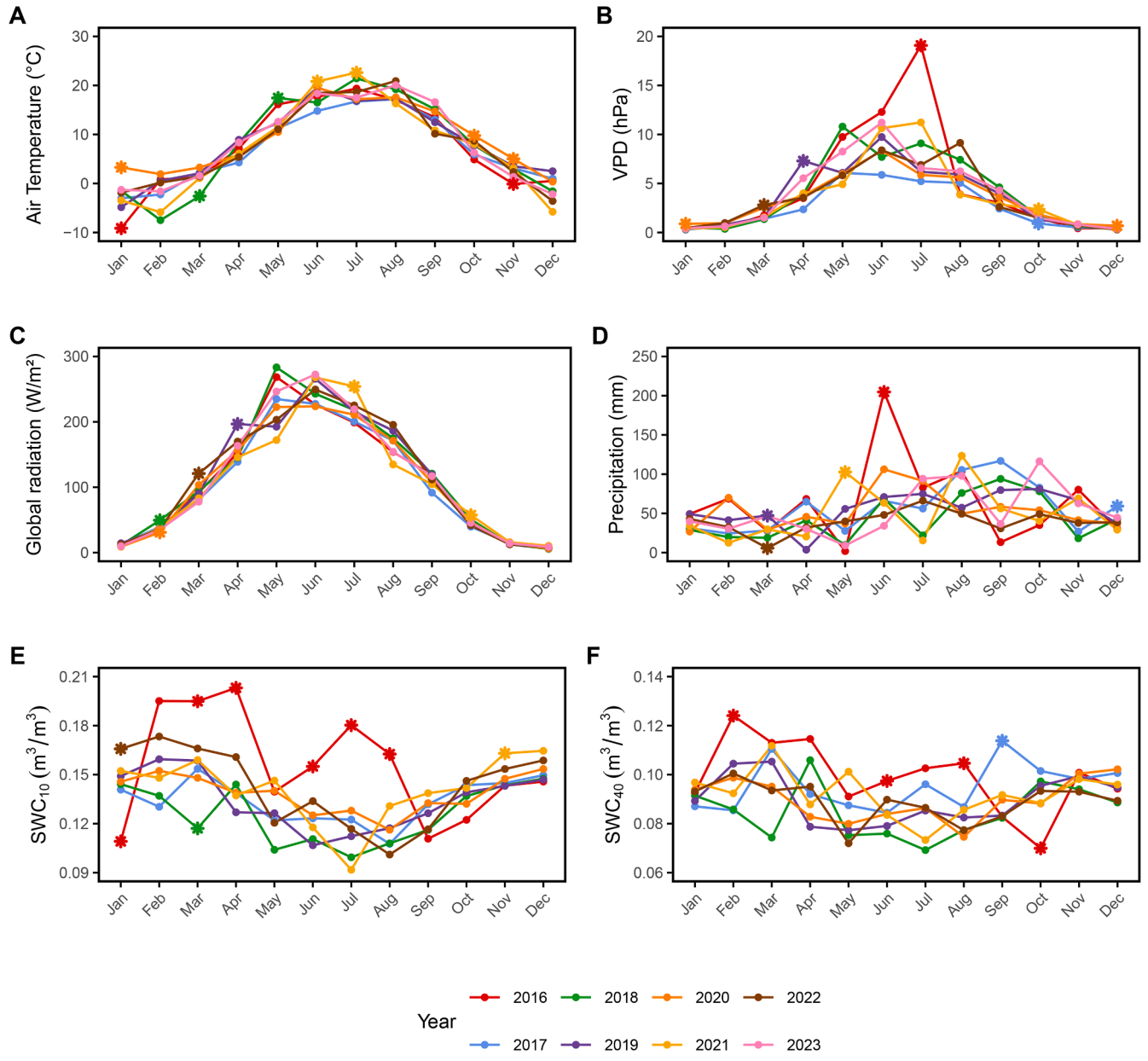

Fig. 5. Monthly dynamics of environmental factors: average air temperature (A), average vapor pressure deficit (VPD, B), average global radiation (C), sums of precipitation (D), average soil water content at 10 cm depth (SWC_{10}, E), average soil water content at 40 cm depth (SWC_{40}, F). Asterisks-shaped markers indicate anomalous months identified based on the interquartile range (IQR) criterion (values below $Q_1 - 1.5 \times IQR$ or above $Q_3 + 1.5 \times IQR$) for the respective variable.

and 2022.

The increase in R_{eco} in the autumn (September – November) of 2020 was one of the main reasons for the neutral annual net carbon balance. However, R_{eco} temperature sensitivity (Q_{10}) of this period was the lowest compared to other years, while F_{10} was the highest (Fig. 8). The absence of low temperature measurements in autumn 2020 noticeably influenced the shape of the temperature response curve. In 2020, air temperatures in October and November were statistically significant anomaly, exceeding the IQR-based threshold for air temperature (Fig. 5A) and representing the warmest autumn months since 2004 (Appendix 4). Although September was also warm, it was not the IQR-based anomaly or warmest over the past 19 years. We made F_{10} and Q_{10} models only for October and November data (Appendix 6).

The eight-year average autumn F_{10} was 2.89 μmol m^{-2} s^{-1}. The highest F_{10} was observed in autumn 2020 and 2021 (+9.3 % and +8.3 % respectively), and the lowest was observed in 2019 (−13.2 %). These results indicate that in 2020 and 2021, night-time ecosystem respiration was less dependent on temperature and more influenced by other environmental factors, whereas in 2019, it was the opposite.

The multi-year average temperature sensitivity (Q_{10}) was 2.18. The highest Q_{10} was in 2016 and 2017 (+27.1 % and +19.3 %, respectively) and the lowest in 2020 (−23.4 %). This confirms that autumn 2020 had significantly lower temperature sensitivity for night-time ecosystem respiration, while the autumns of 2016 and 2017 were more sensitive to temperature increases.

However, models without September data, demonstrated that F_{10} and Q_{10} coefficients are close to the values of other years, indicating a significant impact on September data (Appendix 6). We claim that, as predicted by the random forest model (Fig. 7), air temperature was a primary driver of the increased autumn R_{eco}.

3.4. The maximum photosynthetic capacity dynamics

In our study, we used maximum photosynthetic capacity (GEP_{max})

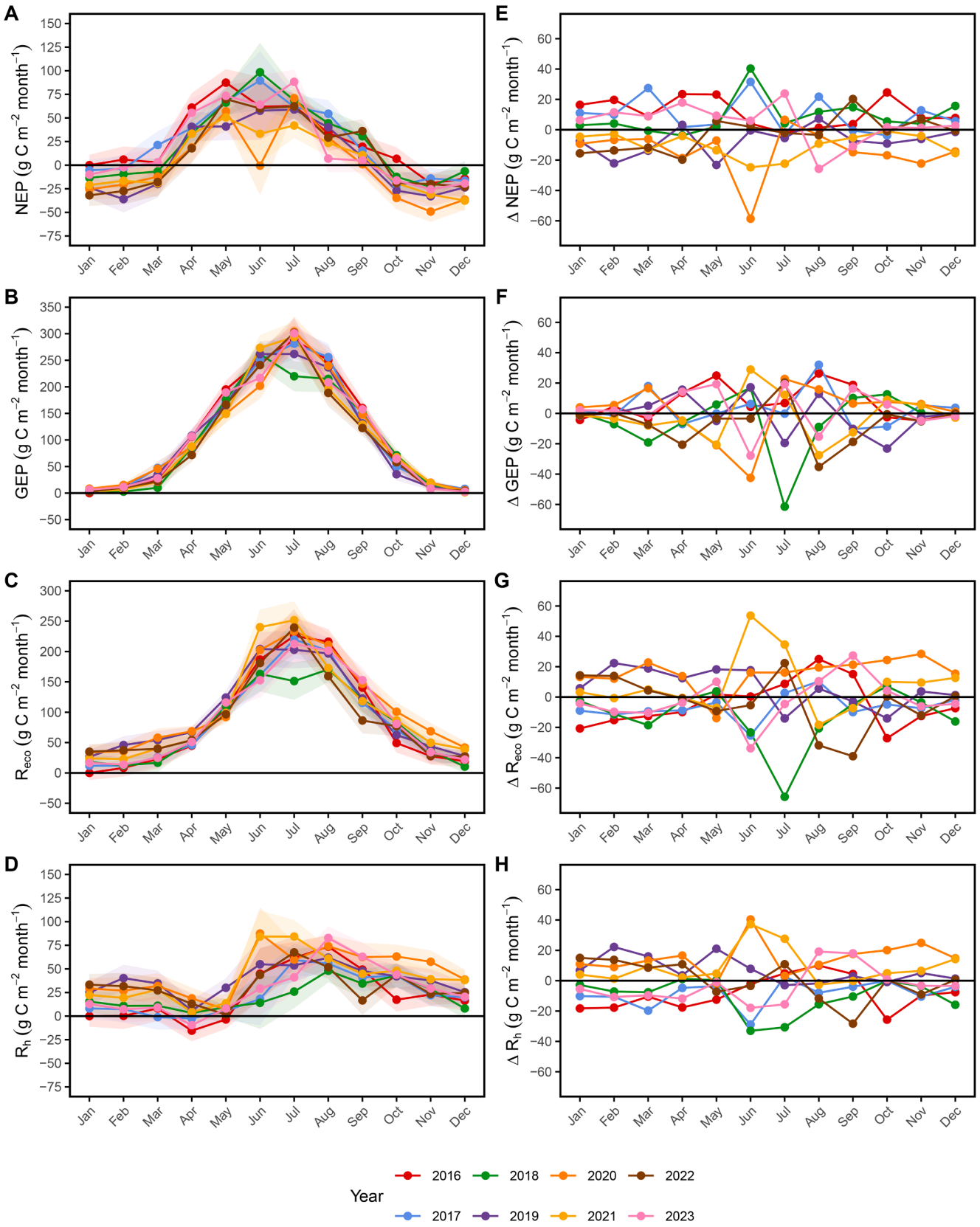

Fig. 6. Monthly dynamics of carbon fluxes and their standard deviations (A-D) and monthly deviations from the eight-year mean (E-H). NEP is Net Ecosystem Production, GEP is Gross Ecosystem Production, R_{eco} is Ecosystem Respiration and R_h is Heterotrophic Respiration.

Table 3
Most pronounced monthly deviations (%) from the eight-year mean in NEP (net ecosystem production), GEP (gross ecosystem production), R_{eco} (ecosystem respiration), and R_h (heterotrophic respiration). Months were identified using an IQR-based outlier criterion (values below $Q_1 - 1.5 * IQR$ or above $Q_3 + 1.5 * IQR$) for at least one variable.

Month and year	NEP (%)	GEP (%)	R_{eco} (%)	R_h (%)
October 2016	−137.8	−4.4	−35.5	−59.7
March 2017	−452.3	61.5	−26.8	−105.7
July 2018	6.7	−21.8	−30.3	−54.2
May 2019	−36.1	−2.9	17.2	234.7
October 2019	51	−39.5	−18.4	−2
June 2020	−101	−17.4	8.7	85.7
October 2020	94.5	12.9	31.9	46.7
November 2020	82.9	45.9	70.6	76.4
June 2021	−42.7	11.8	28.8	79
July 2021	−34.7	4.3	15.9	48.8
September 2022	127.7	−13.3	−31.1	−63.1
July 2023	37	6.8	−2.1	−27.5
August 2023	−78.7	−6.9	5.4	30.1

dynamics as a forest health and recovery indicator, demonstrating how effectively the forest can assimilate carbon. GEP_{max} displayed a clear pattern throughout the eight years of the study: starting in spring, it constantly increased, reaching a peak at the end of July and early August, followed by a decrease in the autumn months (Fig. 9). The impact of the heatwave in 2018 was clearly noticeable, as GEP_{max} was relatively low in July and August (19.80 and 21.79 μmol m^{-2} s^{-1}), when in other years in the same period was observed photosynthetic capacity peak. We did not observe any major changes in GEP_{max} dynamics in the following years, indicating stable potential carbon assimilation by forest stand after the heatwave.

4. Discussion

Studying the carbon dynamics of hemiboreal forests is crucial for understanding their role in the global carbon cycle and developing forestry strategies. This study helped to understand the carbon dynamics in the old upland hemiboreal coniferous forest, identify the main environmental drivers that has the greatest impact on net annual carbon balance, and discover the absence of legacy effect after the heatwave 2018. Our representative study provides new valuable results and findings based on long-term continuous eddy covariance measurements.

4.1. NEP dynamics in hemiboreal forest: The role of R_{eco} and GEP

The range of annual variability of NEP was similar to boreal forests in the northern hemisphere. During an eight-year study in the upland hemiboreal Soontaga forest, the average annual NEP was 170 ± 42 g C m^{-2} $year^{-1}$. This result is close to the measurements from other studied areas: in Hyytiälä, Finland (boreal, evergreen conifer forest) the NEP was 206 ± 38 g C m^{-2} $year^{-1}$ (Ilvesniemi et al., 2009), in Mekrijärvi (also a boreal, evergreen conifer forest) it was 190 ± 24 g C m^{-2} $year^{-1}$ (Ge et al., 2011), and in the Howland boreal forest in Maine, USA, where the NEP was 188 ± 49 g C m^{-2} $year^{-1}$ as reported by Hollinger et al. (2004). This confirms that NEP in the Soontaga hemiboreal forest is in the same range as other coniferous forests in the boreal zone.

Our eight-year study has shown that there were no significant year-to-year changes in GEP during this period, whereas the changes in R_{eco} from year to year were substantial (Fig. 4). While we recognize that R_{eco} and GEP are derived from NEP data, the interannual variability patterns suggest that respiration contributed more to the observed NEP variability. Similar findings were reported by Hadden & Grelle (2016) in the boreal forest of Sweden, where R_{eco} was the main contributor to NEP fluctuations, while GEP remained relatively stable. They also observed that increased R_{eco} levels turned the ecosystem into a carbon source. On the other hand, Froelich et al. (2015) found that in a mixed boreal–temperate forest dominated by deciduous species, an increasing NEP trend was linked to both slightly rising GEP and declining R_{eco}. However, they noted that the forest consists predominantly (approximately 50 %) of red maple (*Acer rubrum*), so for deciduous forests, GEP plays a more crucial role in determining NEP. We assume that the absence of deciduous trees could be one of the reasons for stable annual GEP.

4.2. Spring R_{eco} increase: Investigating the 2019 NEP decline

The year 2019 became the first year when we observed a significant decline in NEP, with NEP being two times lower than the eight-year average as a result of annual R_{eco} enhancement (Fig. 4). While only May was statistically identified as an anomaly, elevated Reco persisted from March to June (Table 3, Fig. 6G). Moreover, in March, May, and June, we inferred increased R_h (Fig. 6D). Close to average or slightly increased GEP over this period and no reduction in photosynthetic capacity indicate, that R_{eco} enhancement was the cause of annual NEP decline. This indicates that NEP declined observed in 2019 was not caused by short-term extreme anomaly, but rather by a moderate increase in R_{eco} over several months.

In contrast with our observations, spring variations in R_{eco} in forest ecosystems were previously found to be less significant compared to GEP, leading to a strong dependence of spring NEP on GEP in temperate and boreal forests (Delpierre et al., 2009; Falge et al., 2002; Welp et al., 2007). We observe this pattern only in April, when modelled R_h does not show significant fluctuations from the average (Fig. 6H), and GEP is 17 % higher compared to the monthly average value (Fig. 6F) and the highest photosynthetic capacity (Fig. 9). This month was also characterized by exceptionally warm, dry, and sunny conditions, the warmest April since 2004 (Appendix 4), even though air temperature remained within the standard range for this month. In contrast, both VPD and Rg exceeded the outlier threshold (Fig. 5B and 5C), indicating all together highly favourable conditions for photosynthesis in coniferous forest ecosystems.

Previous studies demonstrated R_h increase with rising air temperatures (Dalias et al., 2001; Wang et al., 2014; Tremblay et al., 2018) and with the presence of available organic matter and nitrogen availability (Shahbaz et al., 2022). M. Zhang et al. (2022) found that soil respiration was consistently lower at high SWC in temperate forest. In our study, the random forest analysis (Fig. 7) showed that in 2019, air temperature was the most important predictor of ecosystem respiration, with soil moisture also playing a notable role. The combination of moderately elevated air temperatures, sufficient soil water, and high radiation likely created conditions favourable for microbial decomposition. These processes outweighed the gains from photosynthesis, leading to a reduced carbon sink during this period.

4.3. From carbon sink to carbon neutral: The role of autumn R_{eco}

The shift from net carbon sink to carbon-neutral in 2020 was primarily linked to elevated autumn R_{eco}, while GEP remained near average. Autumn 2020 was the warmest on record in the last 19 years (Appendix 5), with October and November air temperatures significantly exceeding the IQR threshold. These conditions likely promoted microbial activity and enhanced R_h, shifting the annual carbon balance close to zero.

F_{10} values in 2020 were the highest observed, while Q_{10} values were the lowest, suggesting that respiration was less sensitive to temperature increases once conditions were already warm (Fig, 8). September appeared less influenced by air temperature, but October and November R_{eco} were strongly temperature-driven. Warmer temperatures, coupled with sufficient soil moisture, likely extended the decomposition period, amplifying autumn R_{eco} and reducing annual NEP. Similar findings from boreal forests attribute autumn NEP reductions to increased R_{eco} under warmer conditions (Piao et al., 2008; Ueyama et al., 2014; Vesala et al.,

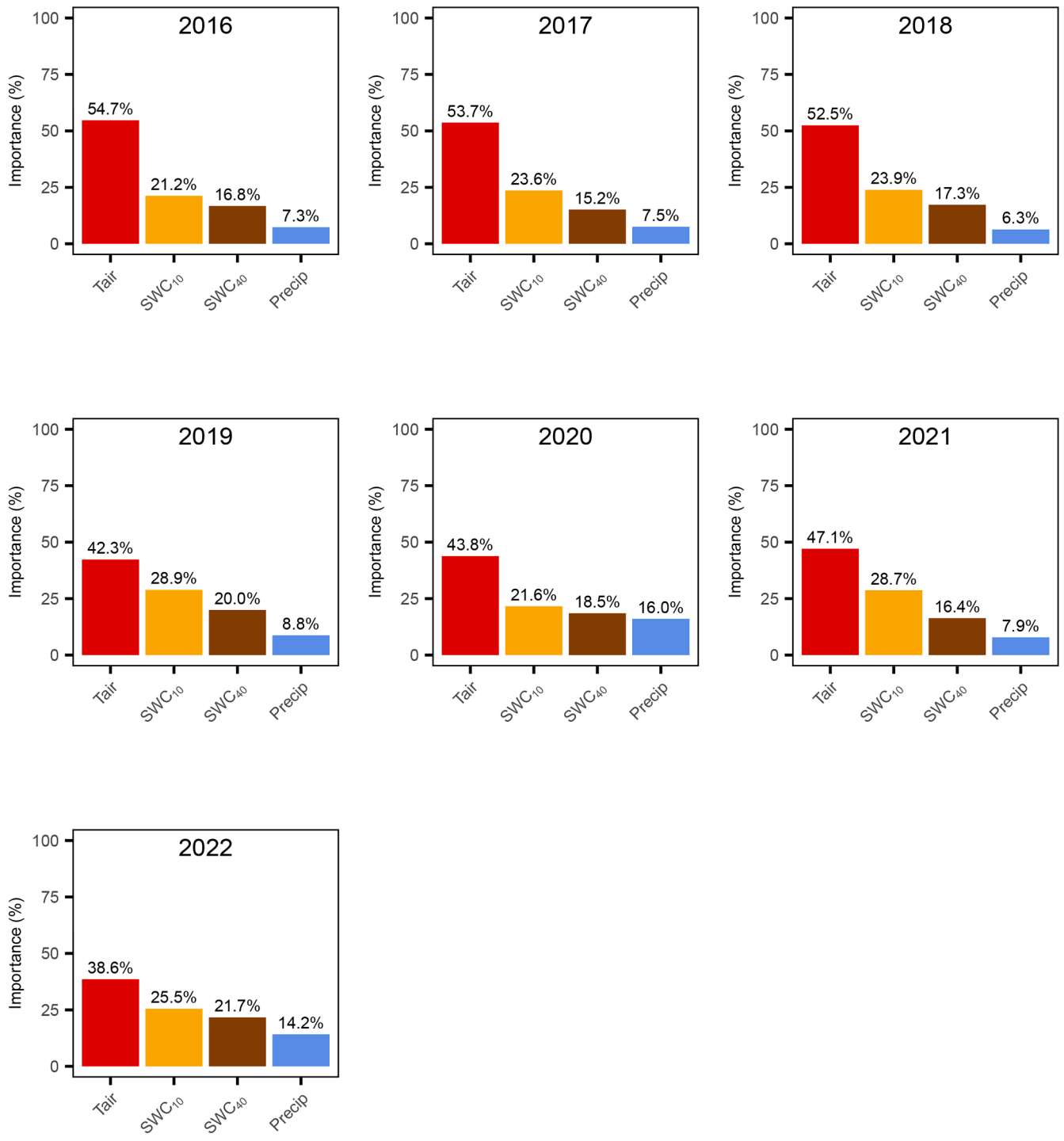

Fig. 7. Importance of meteorological variables: Air temperature (Tair), soil water content at depths of 10 and 40 cm (SWC_{10}, SWC_{40}) and precipitation (Precip) obtained from random forest models.

2010). However, in our study, we did not observe a general trend of increasing autumn temperatures as reported in the paper by Ueyama et al. (2014). On the other hand, Hadden & Grelle (2016) found that a boreal forest emitted more CO_2 in autumn and spring at lower temperatures (from −5 to 10 °C). They linked this not to a general warming trend but to internal changes in the forest ecosystem. In our study, we observed similar patterns; however, in the absence of dead biomass estimates, so we can't directly confirm this. Vesala et al. (2010) found that in a warming climate, the temporal distribution of organic matter decomposition may change throughout the year, but the total volume of decomposition may remain unchanged. Easily decomposable carbon would be exhausted by autumn, resulting in lower soil CO_2 emissions in spring. However, in the spring of 2021, we observed a different pattern, with R_{eco} from January to May being close to their monthly averages.

Our study demonstrated that the old upland coniferous Soontaga forest's carbon dynamics were significantly influenced by a single warm autumn of 2020, which potentially boosted R_h. If single autumn warmings occur more frequently due to the predicted warming in the boreal zone, increased R_h may decrease annual NEP significantly or turn the upland coniferous forest into a carbon source, as was observed in previous studies (Piao et al., 2008; Ueyama et al., 2014). Additionally, our study raises the question about the quantity of easily decomposable

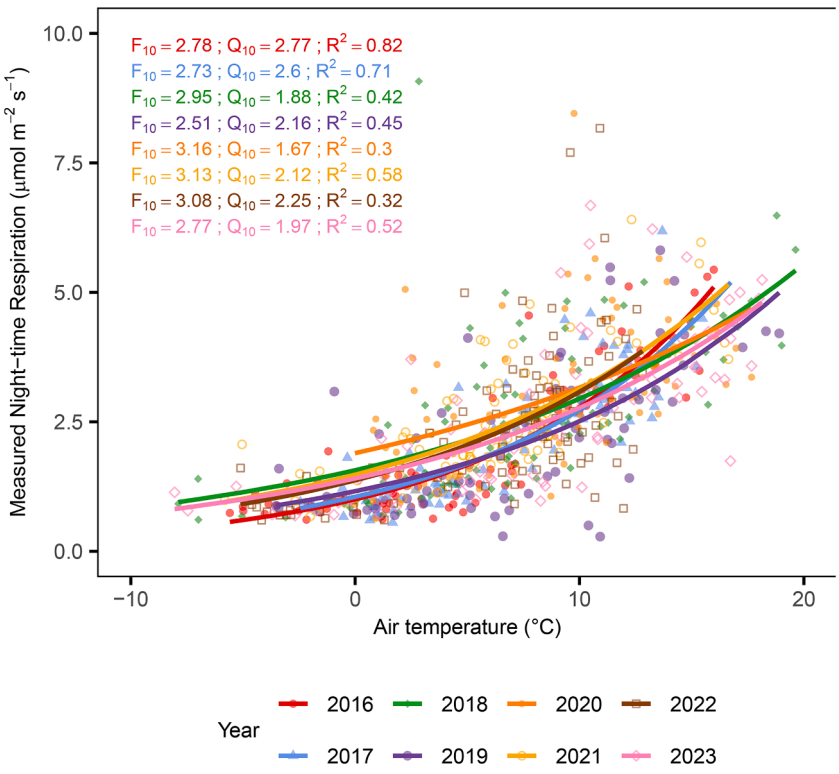

Fig. 8. Temperature response of autumn (September – November) measured R_{eco}. The curves are Q_{10} respiration model (Eq. (5)) fits with parameters marked by the corresponding colours.

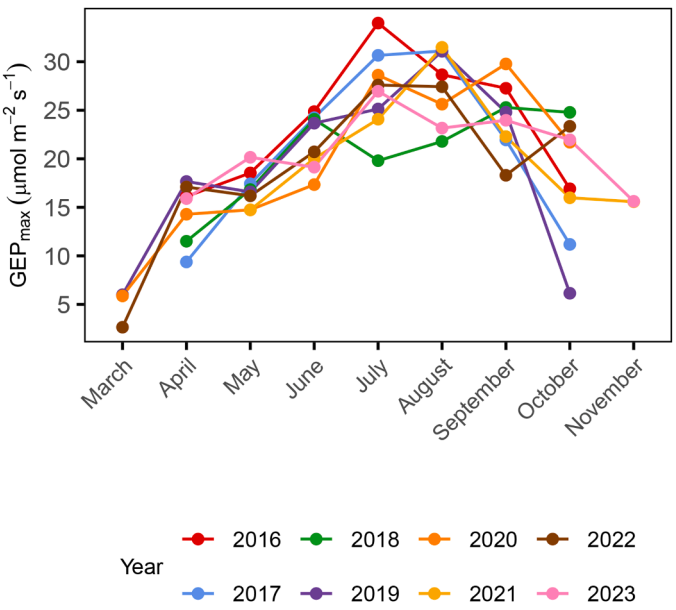

Fig. 9. Monthly dynamics of maximum photosynthetic capacity (GEP_{max}) from 2016 to 2023.

carbon in the upland hemiboreal forest and its exhaustion after a single warm autumn, as observed in the study by Vesala et al. (2010). In our study, we did not find any evidence that the amount of easily decomposable carbon would be low after a warm autumn. We hypothesize two possibilities: either the quantity of easily decomposable carbon is too large to be significantly reduced by one warm event, or the amount of decomposable carbon increases during winter. However, without further in-depth and focused research, we cannot confidently claim this.

4.4. *Summer carbon fluxes dynamics: Temperature and moisture impact*

We observed three summer months (June 2020, and June and July 2021) when R_{eco}, not GEP, was the main contributor to NEP, an unusual pattern for boreal and hemiboreal forests in the Northern Hemisphere (Krishnan et al., 2009).

In June 2020, low GEP combined with exceptionally high R_h estimate, nearly double that of other Junes, led to negative NEP (Fig. 6A). Reduced radiation early in the month likely limited photosynthesis, while subsequent brief period of heat and increased precipitation favoured microbial decomposition, rapidly increasing R_h. von Buttlar et al. (2018) and Arain et al. (2022) found that short periods of heat (first 18 days) stimulate an increase in R_{eco}. Moreover, increased precipitation and warm weather in the second half of the month could create optimal conditions for the decomposition of organic matter by soil microorganisms, leading to a sharp increase in R_h (Borken et al., 2003; Yu et al., 2015). Based on this, we assume that in June 2020, high air temperatures and water availability created optimal conditions for enhanced R_h. However, with rapidly increasing temperatures, R_{eco} increased at a faster rate than GEP (Yvon-Durocher et al., 2010). As a result, R_{eco} became the main contributor to NEP. This observation is particularly significant because, when combined with the warm autumn described in subchapter 4.3, it demonstrates that multiple unusual events can collectively shift an upland hemiboreal forest to a carbon-neutral state. The autumn months together accounted for nearly a quarter of the annual R_{eco}, with June alone contributing approximately one-sixth of the total.

In June and July 2021, both GEP and R_{eco} increased under record-high air temperatures, but the rise in R_{eco} outpaced that of GEP, lowering NEP (Fig. 6B and 6C). Sufficient soil moisture in June supported high ecosystem activity, but by July, precipitation deficits caused moderate drought stress, proportionally reducing both GEP and R_{eco}.

Our results clearly demonstrate that warmer summers, much like warmer autumns, can shift the carbon dynamics of the upland

hemiboreal forests to a carbon source direction. Because summer months account for a larger share of annual R_{eco} than autumn, further warming may have stronger impacts, particularly under fluctuating soil moisture conditions that constrain photosynthesis as well as respiration. While we did not observe a significant trend of increasing summer temperatures, summer warming could pose a threat of amplified drought or heat stress.

4.5. Heatwave 2018: The resilience of a hemiboreal forest

From the middle of July to the beginning of August 2018, we observed a heatwave comparable in intensity to well-documented events in 2003 and 2010 in Northern Europe (Bastos et al., 2020; Krasnova et al., 2022). It significantly impacted the carbon dynamics of the Soontaga forest but did not reduce annual carbon uptake. Annual NEP (271 ± 10 g C m^{-2} $year^{-1}$) exceeded the study average (167 ± 42 g C m^{-2} $year^{-1}$), despite concurrent reductions in both GEP and R_{eco}. A similar finding was previously reported by Lindroth et al. (2020) for pine forests in Finland and Sweden: the 56-year-old pine forest stand in Hyytiälä had an NEP of 297 g C m^{-2} $year^{-1}$, and the 90-year-old pine forest stand in Rosinedal had an NEP of 234 g C m^{-2} $year^{-1}$, with reductions observed in both R_{eco} and GEP. The annual NEP dynamics of Hyytiälä and Rosinedal were similar to ours, indicating that our data reflected the carbon dynamics in the boreal climate zone in 2018.

Seasonally, exceptionally high NEP in June was followed by subsequent reductions of GEP and R_{eco} in July and August due to extreme heat, that was not reflected in monthly NEP. Smith et al. (2020) found that an increase in NEP in June compensated for the reduction in NEP in July 2018 on a seasonal scale. On the other hand, Mamkin et al. (2022) reported that during the summer period of 2018, in the nemoral spruce forest in Russia, there was an increase in GEP and a decrease in R_{eco}, which led to an increase in net CO_2 uptake. According to their findings, the main drivers of this phenomenon were higher SWC and different VPD dynamics. Overall, our observations align with other studies during the 2018 heatwave period, with some variations depending on the specific characteristics of each forest stand.

Heatwaves produce immediate, post-heatwave, legacy, and cumulative effects, which each uniquely influence the ecosystem's carbon cycle (Qu et al., 2024). Heatwaves typically bring drought, but understanding of drought impacts is complicated because not all responses are immediately visible (Kannenberg et al., 2020). From previous studies, we know that the legacy effects of drought can be noticeable in deciduous trees through hydraulic damage and dieback (Anderegg et al., 2013). Moreover, Schuldt et al. (2020) demonstrated in their study that following the heatwave of 2018, Norway spruce, Scots pine, and silver fir (*Abies alba*) were among the most affected species due to hydraulic failure. This makes the situation especially intriguing because Galiano et al. (2011) demonstrated in their study that Scots pine trees take a long time to recover from a drought episode. Furthermore, trees, after a drought event, become more vulnerable to pests living on foliage due to the weakening of their protective mechanisms (Jactel et al., 2012). Similarly to the study by Schuldt et al. (2020), the Soontaga forest mainly consists of Scots pine with a second layer of Norway spruce. In July, we also observed the second-lowest SWC at a depth of 10 cm and the lowest result at a depth of 40 cm (Fig. 5E and 5F), which could indicate drought conditions. However, despite this, during the next 5 years, we did not observe hydraulic damage or pest infestation increase that could have triggered increased tree mortality.

Heatwaves impact often result in GEP reduction (Ciais et al., 2005; Lindroth et al., 2020; Xu et al., 2020; Yan et al., 2023) due to the influence of extreme air temperatures on plant growth, reproduction, and survival (Breshears et al., 2021). The maximum photosynthetic capacity could be used as a good indicator of a forest ecosystem health (Xia et al., 2015). Our study results demonstrate a decrease in GEP_{max} in July and August of 2018, indicating the negative impact of the 2018 heatwave on the ecosystem's carbon uptake capacity (Fig. 9). However, by September, it recovered to its average September value. In the following years, the GEP_{max} dynamics remain unchanged, following pre-heatwave patterns and values with minor deviations. This rapid recovery highlights the resilience of the Scots pine-dominated hemiboreal forest to short-term climatic extremes, in contrast to the persistent post-drought effects documented for other coniferous species in Europe (Schuldt et al., 2020; Galiano et al., 2011).

4.6. Carbon sequestration: The importance of tree age in hemiboreal forests

There is no consensus regarding the sink strength of old forests. A study by Luyssaert et al. (2008) found that old-growth forests can continue to accumulate carbon, controversially to the long-held belief of their carbon neutrality. However, Gundersen et al. (2021) pointed out an overestimation in the quantification of old forests' carbon sequestration. Previously, Carey et al. (2001) have shown that old coniferous forests have higher productivity as carbon sinks than predicted by models. Leverett et al. (2021) found that older eastern white pine forests are very effective at capturing and holding carbon. However, studies by Chapin et al. (2011) and Hadden & Grelle (2017) concluded that as forests mature and growth slows, there is a decrease in carbon uptake.

We found that in the old hemiboreal coniferous forest, the positive NEP in 7 out of 8 years is ensured by the very stable GEP from year to year. Moreover, in 2020, when NEP became negative, GEP was still close to average. On the one hand, the stability of GEP can be attributed to the mosaic of age classes within the footprint. While mature and overmature stands (43 % of area) may exhibit declining productivity, middle-aged and premature stands (48 % of area) continue to increase GEP, offsetting losses from older trees. Furthermore, younger Norway spruces growing beneath older Scots pines in mature stands also contribute to this compensation, stabilizing stand-level GEP over time. On the other hand, it's important to note that the tower is located in an overmature forest stand, which covers half of the total area of this age group, making its influence potentially very significant. There is evidence that sustained NEP is primarily explained by the stable mean GEP of trees aged 100–200 years (Peichl et al., 2023; Stokland, 2021). Age-structure diversity could be one of the key mechanisms maintaining carbon sequestration in old hemiboreal forests, buffering declines in productivity of older trees.

5. Conclusion

Over the eight-year observation period (2016–2023), the old hemiboreal upland coniferous forest acted as a consistent net carbon sink, with the exception of a single carbon-neutral year 2020. Mean annual NEP (170 ± 42 g C m^{-2} yr^{-1}) was well within the range reported for boreal coniferous forests, underscoring the important role of old-growth hemiboreal forests in long-term carbon sequestration.

Interannual variability in NEP was primarily driven by changes in R_{eco}, while GEP remained comparatively stable. R_{eco} was primarily controlled by air temperature, with soil water content exerting a secondary influence. Anomalously warm conditions, particularly the exceptionally warm autumn of 2020 and concurrent water limitation in June-July 2021, considerably enhanced R_{eco} and offset annual net carbon uptake, highlighting the sensitivity of the carbon balance to temperature variability.

Despite such these natural disturbances, the forest displayed a high degree of resistance and resilience to climatic extremes. The 2018 heatwave, although temporarily reducing photosynthetic capacity, did not diminish annual carbon uptake, and no legacy effects were detected in the subsequent years. This capacity to maintain carbon sequestration under variable climatic conditions highlights the functional stability of old hemiboreal coniferous forests in the face of increasing rate of climate extremes.

CRediT authorship contribution statement

Svyatoslav Rogozin: Writing – review & editing, Writing – original draft, Visualization, Investigation, Formal analysis, Data curation. **Alisa Krasnova:** Writing – review & editing, Supervision, Methodology, Investigation, Data curation, Conceptualization. **Ülo Mander:** Writing – review & editing, Supervision, Funding acquisition, Conceptualization. **Veiko Uri:** Writing – review & editing, Data curation. **Kaido Soosaar:** Writing – review & editing, Supervision, Funding acquisition, Conceptualization.

Declaration of competing interest

The authors declare that they have no known competing financial interests or personal relationships that could have appeared to influence the work reported in this paper.

Acknowledgements

This study was supported by the Ministry of Education and Research of Estonia (IUT2-16); the European Union through the European Regional Development Fund (BioAtmos) (3.2.0802.11-0043), the Estonian Research Infrastructures Roadmap Project Estonian Environmental Observatory (3.2.0304.11-0395) and the Centre of Excellence ENVIRON (TK107), Centre of Excellence EcolChange (TK131) and Center of Excellence AgroCropFuture (TK200). This work was also supported by the European Union Horizon programme under grant agreement No 101079192 (MLTOM23003R) and the European Research Council (ERC) under grant agreement No 101096403 (MLTOM23415R).

Appendix 1

Table 4
Yearly u* thresholds, data metrics, and NEE gap-fill uncertainty (RMSE and MBE in g C $year^{-1}$).

Year	Available measured before data filtering	Friction velocity ($m\ s^{-1}$)	Spikes	Available quality-controlled data	NEE RMSE (g C $year^{-1}$)	NEE MBE (g C $year^{-1}$)
2016	92.70 %	0.19	0.79 %	77.16 %	6.89	18.68
2017	93.16 %	0.2	0.85 %	77.52 %	6.8	19.70
2018	86.99 %	0.32	1.03 %	59.82 %	6.48	14.73
2019	90.05 %	0.31	1.10 %	66.95 %	6.5	4.12
2020	95.53 %	0.17	0.83 %	84.53 %	7.56	12.96
2021	96.14 %	0.2	1.16 %	81.87 %	6.97	8.64
2022	86.29 %	0.22	0.78 %	69.76 %	8.82	2.70
2023	82.05 %	0.21	0.74 %	68.18 %	6.55	−1.77

Appendix 2

Table 5
Annual NEP, R_{eco}, and GEP (g C $year^{-1}$ ± Uncertainty) with fixed (0.2 m s^{-1}) and varying u* thresholds (0.19–0.31 m s^{-1}; Appendix 1).

Year	$NEP_{VaryingUstar}$	$NEP_{FixedUstar}$	$GEP_{VaryingUstar}$	$GEP_{FixedUstar}$	$R_{ecoVaryingUstar}$	$R_{ecoFixedUstar}$
2016	309 ± 14	305 ± 13	1357 ± 16	1364 ± 21	1049 ± 26	1059 ± 24
2017	288 ± 9	287 ± 9	1313 ± 8	1311 ± 7	1025 ± 10	1025 ± 9
2018	271 ± 10	223 ± 16	1216 ± 24	1247 ± 27	946 ± 34	1024 ± 36
2019	84 ± 6	57 ± 10	1262 ± 28	1230 ± 30	1178 ± 35	1173 ± 36
2020	−2 ± 5	2 ± 7	1290 ± 33	1288 ± 30	1293 ± 40	1286 ± 43
2021	49 ± 3	50 ± 3	1248 ± 14	1246 ± 14	1198 ± 18	1196 ± 17
2022	137 ± 6	132 ± 10	1198 ± 22	1198 ± 20	1061 ± 22	1066 ± 26
2023	222 ± 8	217 ± 8	1301 ± 16	1303 ± 17	1078 ± 22	1087 ± 24

Appendix 3

Table 6
Performance metrics of Random Forest models by year.

Year	R^2	MAE	RMSE
2016	0.48	20.21	28.72
2017	0.60	16.05	22.25
2018	0.49	18.27	26.05
2019	0.30	20.42	28.18
2020	0.33	24.52	31.95
2021	0.43	21.53	28.20
2022	0.28	21.59	28.54

Appendix 4

Table 7
Monthly mean air temperatures (°C) from 2004 −2023.

Year	January	February	March	April	May	June	July	August	September	October	November	December
2004	−7.6	−4.2	0.1	6.1	10.6	13.8	16.9	17.5	12.2	6.1	−0.5	0.0
2005	−1.6	−7.6	−6.0	5.2	11.2	14.8	18.6	16.5	13.2	7.1	2.9	−3.9
2006	−6.4	−9.2	−4.2	5.9	11.3	16.7	19.0	17.1	14.0	8.3	2.6	3.2
2007	−1.7	−10.2	4.5	5.5	12.3	16.3	17.0	18.2	11.4	6.9	0.0	0.8
2008	−1.1	0.9	0.7	7.4	10.7	14.6	16.6	16.1	10.1	8.5	2.5	−0.8
2009	−3.1	−4.7	−1.0	6.2	11.8	14.2	17.3	15.8	13.1	4.3	2.6	−4.8
2010	−13.7	−7.5	−1.3	6.4	12.3	15.0	22.6	18.4	11.3	4.5	0.5	−8.0
2011	−4.3	−10.8	−1.2	6.8	11.7	17.7	20.5	16.6	12.8	7.4	3.7	1.6
2012	−5.2	−10.5	0.1	5.3	12.0	13.9	18.3	15.2	12.4	6.0	2.7	−6.5
2013	−7.1	−3.0	−7.0	4.0	15.0	18.2	17.9	17.2	11.3	7.2	4.1	1.7
2014	−8.0	0.0	2.7	6.9	12.4	13.7	19.6	16.8	12.4	5.6	1.5	−1.3
2015	−1.5	−0.8	3.0	5.8	10.7	14.6	16.1	17.0	12.8	4.8	3.7	2.4
2016	−9.1	0.8	1.2	7.2	16.1	17.7	19.4	17.0	13.5	4.9	−0.1	0.5
2017	−3.0	−2.3	2.2	4.3	11.3	14.8	16.7	17.2	13.0	5.9	3.1	1.0
2018	−1.5	−7.5	−2.6	8.3	17.4	16.5	21.4	19.2	15.1	7.8	3.0	−1.6
2019	−4.8	0.6	2.1	8.9	12.4	19.6	16.9	17.3	12.5	7.8	3.5	2.5
2020	3.3	1.9	3.3	5.9	10.5	19.5	17.2	17.6	14.7	9.8	5.0	0.4
2021	−3.5	−5.9	1.1	6.1	11.6	20.8	22.6	16.3	10.8	8.0	3.2	−5.8
2022	−1.9	0.2	1.5	5.4	11.0	18.5	18.7	20.9	10.1	8.7	2.3	−3.6
2023	−1.3	−1.6	1.6	8.4	12.6	18.4	17.5	20.0	16.6	6.3	1.4	−2.2

Appendix 5

Table 8
Seasonal mean air temperatures (°C) from 2004 −2023.

Year	Winter (Dec, Jan, Feb)	Spring (Mar, Apr, May)	Summer (Jun, Jul, Aug)	Autumn (Sep, Oct, Nov)
2004	−3.9	5.6	16.0	5.9
2005	−4.4	3.5	16.6	7.7
2006	−4.1	4.3	17.6	8.3
2007	−3.7	7.4	17.1	6.1
2008	−0.4	6.3	15.8	7.0
2009	−4.2	5.7	15.8	6.7
2010	−9.7	6.0	18.7	5.4
2011	−4.5	5.8	18.2	8.0
2012	−7.4	5.8	15.8	7.0
2013	−2.8	4.0	17.8	7.5
2014	−3.1	7.3	16.7	6.5
2015	0.0	6.5	15.9	7.1
2016	−2.6	8.0	18.0	6.1
2017	−1.4	5.9	16.2	7.4
2018	−3.5	7.7	19.1	8.6
2019	−0.6	7.8	17.9	8.0
2020	1.9	6.5	18.1	9.8
2021	−5.0	6.3	19.9	7.3
2022	−1.8	6.0	19.3	7.1
2023	−1.7	7.5	18.6	8.1

Appendix 6

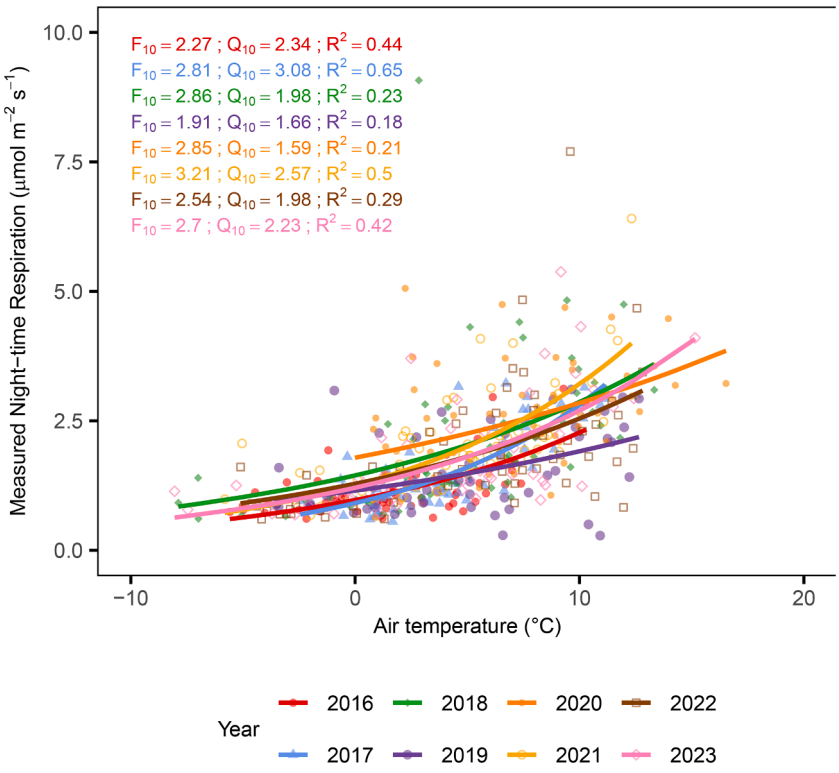

Fig. A6. October and November measured night-time respiration at 10 °C and temperature sensitivity model and their coefficients.

Appendix 7

Table 9
Mean daily air temperature and standard deviation (°C) during 15 Jul–5 Aug for each year 2016–2023.

Year	Mean air temperature (°C) ± standard deviation
2016	19.5 ± 2
2017	17.6 ± 1.7
2018	24.2 ± 1.6
2019	17.9 ± 3.9
2020	17.8 ± 2.7
2021	20.1 ± 3.2
2022	18.4 ± 3.1
2023	18.0 ± 1.9

Data availability

Data will be made available on request.

References

Ahti, T., Hämet-Ahti, L., Jalas, J., 1968. Vegetation zones and their sections in northwestern Europe. Ann. Bot. Fenn. 5 (3), 169–211.

Anderegg, W.R.L., Schwalm, C., Biondi, F., Camarero, J.J., Koch, G., Litvak, M., Ogle, K., Shaw, J.D., Shevliakova, E., Williams, A.P., Wolf, A., Ziaco, E., Pacala, S., 2015. Pervasive drought legacies in forest ecosystems and their implications for carbon cycle models. Science 349 (6247), 528–532. 10.1126/science.aab1833.

Arain, M.A., Xu, B., Brodeur, J.J., Khomik, M., Peichl, M., Beamesderfer, E., Restrepo-Couple, N., Thorne, R., 2022. Heat and drought impact on carbon exchange in an age-sequence of temperate pine forests. Ecol. Proc. 11 (1), 7. https://doi.org/10.1186/s13717-021-00349-7.

Baldocchi, D., Kelliher, F. M., Black, T. A., & Jarvis, P. (2000). Climate and vegetation controls on boreal zone energy exchange. Glob. Chang. Biol., *6*(S1), 69–83. 10.1046/j.1365-2486.2000.06014.x.

Barba, J., Cueva, A., Bahn, M., Barron-Gafford, G.A., Bond-Lamberty, B., Hanson, P.J., Jaimes, A., Kulmala, L., Pumpanen, J., Scott, R.L., Wohlfahrt, G., Vargas, R., 2018. Comparing ecosystem and soil respiration: review and key challenges of tower-based and soil measurements. Agric. For. Meteorol. 249, 434–443. https://doi.org/10.1016/j.agrformet.2017.10.028.

Barr, A.G., Black, T.A., Hogg, E.H., Griffis, T.J., Morgenstern, K., Kljun, N., Theede, A., Nesic, Z., 2007. Climatic controls on the carbon and water balances of a boreal aspen forest, 1994–2003. Glob. Chang. Biol. 13 (3), 561–576. 10.1111/j.1365-2486.2006.01220.x.

Barr, A., Black, T.A., McCaughey, H., 2009. Climatic and Phenological Controls of the Carbon and Energy Balances of Three Contrasting Boreal Forest Ecosystems in Western Canada. In: Noormets, A. (Ed.), *Phenology of Ecosystem Processes: Applications in Global Change Research*. Springer, pp. 3–34. 10.1007/978-1-4419-0026-5_1.

Barriopedro, D., Fischer, E.M., Luterbacher, J., Trigo, R.M., García-Herrera, R., 2011. The Hot Summer of 2010: Redrawing the Temperature Record Map of Europe. Science 332 (6026), 220–224. 10.1126/science.1201224.

Bastos, A., Fu, Z., Ciais, P., Friedlingstein, P., Sitch, S., Pongratz, J., Weber, U., Reichstein, M., Anthoni, P., Arneth, A., Haverd, V., Jain, A., Joetzjer, E., Knauer, J., Lienert, S., Loughran, T., McGuire, P.C., Obermeier, W., Padrón, R.S., Zaehle, S., 2020. Impacts of extreme summers on European ecosystems: a comparative analysis

of 2003, 2010 and 2018. Philosophic. Transac. Royal Soc. B. 375 (1810), 20190507. https://doi.org/10.1098/rstb.2019.0507.
Bergeron, O., Margolis, H.A., Black, T.A., Coursolle, C., Dunn, A.L., Barr, A.G., Wofsy, S. C., 2007. Comparison of carbon dioxide fluxes over three boreal black spruce forests in Canada. Glob. Chang. Biol. 13 (1), 89–107. 10.1111/j.1365-2486.2006.01281.x.
Bonan, G., 2008. Forests and Climate Change: Forcings, Feedbacks, and the Climate Benefits of Forests. Science (New York, N.Y.) 320, 1444–1449. 10.1126/science.1155121.
Borken, W., Davidson, E.A., Savage, K., Gaudinski, J., Trumbore, S.E., 2003. Drying and wetting effects on carbon dioxide release from organic horizons. Soil Sci. Soc. Am. J. 67 (6), 1888–1896. https://doi.org/10.2136/sssaj2003.1888.
Braybrook, C.A., Scott, N.A., Treitz, P.M., Humphreys, E.R., 2021. Interannual variability of summer net ecosystem CO2 exchange in high arctic Tundra. J. Geophysic. Res. 126 (8), e2020JG006094. https://doi.org/10.1029/2020JG006094.
Breiman, L., 2001. Random forests. Mach. Learn. 45 (1), 5–32. https://doi.org/10.1023/A:1010933404324.
Breshears, D.D., Fontaine, J.B., Ruthrof, K.X., Field, J.P., Feng, X., Burger, J.R., Law, D.J., Kala, J., Hardy, G.E., St, J., 2021. Underappreciated plant vulnerabilities to heat waves. New Phytologist. 231 (1), 32–39. https://doi.org/10.1111/nph.17348.
Carey, E.V., Sala, A., Keane, R., Callaway, R.M., 2001. Are old forests underestimated as global carbon sinks? Glob. Chang. Biol. 7 (4), 339–344. https://doi.org/10.1046/j.1365-2486.2001.00418.x.
Chan, F.C.C., Altaf Arain, M., Khomik, M., Brodeur, J.J., Peichl, M., Restrepo-Coupe, N., Thorne, R., Beamesderfer, E., McKenzie, S., Xu, B., Croft, H., Pejam, M., Trant, J., Kula, M., Skubel, R., 2018. Carbon, water and energy exchange dynamics of a young pine plantation forest during the initial fourteen years of growth. For. Ecol. Manag. 410, 12–26. 10.1016/j.foreco.2017.12.024.
Chapin, F.S., Matson, P.A., Vitousek, P.M., 2011. Principles of Terrestrial Ecosystem Ecology. Springer. https://doi.org/10.1007/978-1-4419-9504-9.
Chen, J.M., Chen, B., Higuchi, K., Liu, J., Chan, D., Worthy, D., Tans, P., Black, A., 2006. Boreal ecosystems sequestered more carbon in warmer years. Geophys. Res. Lett.33 (10). 10.1029/2006GL025919.
Ciais, P., Reichstein, M., Viovy, N., Granier, A., Ogée, J., Allard, V., Aubinet, M., Buchmann, N., Bernhofer, C., Carrara, A., Chevallier, F., De Noblet, N., Friend, A.D., Friedlingstein, P., Grünwald, T., Heinesch, B., Keronen, P., Knohl, A., Krinner, G., Valentini, R., 2005. Europe-wide reduction in primary productivity caused by the heat and drought in 2003. Nature 437 (7058), 529–533. https://doi.org/10.1038/nature03972.
Dalias, P., Anderson, J.M., Bottner, P., Coûteaux, M.-M., 2001. Temperature responses of carbon mineralization in conifer forest soils from different regional climates incubated under standard laboratory conditions. Glob. Chang Biol. 7 (2), 181–192. https://doi.org/10.1046/j.1365-2486.2001.00386.x.
De Boeck, Dreesen, F.E., Janssens, I.A., Nijs, I., 2010. Climatic characteristics of heat waves and their simulation in plant experiments. Glob. Chang Biol. 16 (7), 1992–2000. 10.1111/j.1365-2486.2009.02049.x.
Delpierre, N., Soudani, K., François, C., Köstner, B., Pontailler, J.-Y., Nikinmaa, E., Misson, L., Aubinet, M., Bernhofer, C., Granier, A., Grünwald, T., Heinesch, B., Longdoz, B., Ourcival, J.-M., Rambal, S., Vesala, T., Dufrêne, E., 2009. Exceptional carbon uptake in European forests during the warm spring of 2007: a data–model analysis. Glob. Chang. Biol. 15 (6), 1455–1474. https://doi.org/10.1111/j.1365-2486.2008.01835.x.
Dixon, R.K., Solomon, A.M., Brown, S., Houghton, R.A., Trexier, M.C., Wisniewski, J., 1994. Carbon Pools and Flux of. For Ecosyst. 263 (5144), 185–190. 10.1126/science.263.5144.185.
Dunn, A.L., Barford, C.C., Wofsy, S.C., Goulden, M.L., Daube, B.C., 2007. A long-term record of carbon exchange in a boreal black spruce forest: Means, responses to interannual variability, and decadal trends. Glob. Chang Biol. 13 (3), 577–590. 10.1111/j.1365-2486.2006.01221.x.
Falge, E., Baldocchi, D., Tenhunen, J., Aubinet, M., Bakwin, P., Berbigier, P., Bernhofer, C., Burba, G., Clement, R., Davis, K.J., Elbers, J.A., Goldstein, A.H., Grelle, A., Granier, A., Guðmundsson, J., Hollinger, D., Kowalski, A.S., Katul, G., Law, B.E., Wofsy, S., 2002. Seasonality of ecosystem respiration and gross primary production as derived from FLUXNET measurements. Agric. For. Meteorol. 113 (1), 53–74. https://doi.org/10.1016/S0168-1923(02)00102-8.
FAO, 2020. Global Forest Resources Assessment 2020: Main report. FAO. https://doi.org/10.4060/ca9825en.
Froelich, N., Croft, H., Chen, J.M., Gonsamo, A., Staebler, R.M., 2015. Trends of carbon fluxes and climate over a mixed temperate–boreal transition forest in southern Ontario, Canada. Agric. For. Meteorol. 211–212, 72–84. https://doi.org/10.1016/j.agrformet.2015.05.009.
Galiano, L., Martínez-Vilalta, J., Lloret, F., 2011. Carbon reserves and canopy defoliation determine the recovery of Scots pine 4 yr after a drought episode. New Phytologist. 190 (3), 750–759. https://doi.org/10.1111/j.1469-8137.2010.03628.x.
Ge, Z.-M., Kellomäki, S., Zhou, X., Wang, K.-Y., Peltola, H., 2011. Evaluation of carbon exchange in a boreal coniferous stand over a 10-year period: an integrated analysis based on ecosystem model simulations and eddy covariance measurements. Agric. For. Meteorol. 151 (2), 191–203. https://doi.org/10.1016/j.agrformet.2010.10.003.
Granier, A., Reichstein, M., Bréda, N., Janssens, I.A., Falge, E., Ciais, P., Grünwald, T., Aubinet, M., Berbigier, P., Bernhofer, C., Buchmann, N., Facini, O., Grassi, G., Heinesch, B., Ilvesniemi, H., Keronen, P., Knohl, A., Köstner, B., Lagergren, F., Wang, Q., 2007. Evidence for soil water control on carbon and water dynamics in European forests during the extremely dry year: 2003. Agric. For. Meteorol. 143 (1), 123–145. 10.1016/j.agrformet.2006.12.004.
Gundersen, P., Thybring, E.E., Nord-Larsen, T., Vesterdal, L., Nadelhoffer, K.J., Johannsen, V.K., 2021. Old-growth forest carbon sinks overestimated. Nature 591 (7851), E21–E23. https://doi.org/10.1038/s41586-021-03266-z.
Hadden, D., Grelle, A., 2016. Changing temperature response of respiration turns boreal forest from carbon sink into carbon source. Agric. For. Meteorol. 223, 30–38. https://doi.org/10.1016/j.agrformet.2016.03.020.
Hadden, D., Grelle, A., 2017. Net CO2 emissions from a primary boreo-nemoral forest over a 10year period. For. Ecol. Manage. 398, 164–173. https://doi.org/10.1016/j.foreco.2017.05.008.
Hickler, T., Vohland, K., Feehan, J., Miller, P.A., Smith, B., Costa, L., Giesecke, T., Fronzek, S., Carter, T.R., Cramer, W., Kühn, I., Sykes, M.T., 2012. Projecting the future distribution of European potential natural vegetation zones with a generalized, tree species-based dynamic vegetation model. Glob. Eco. Bio. 21 (1), 50–63. 10.1111/j.1466-8238.2010.00613.x.
Hoff, J.H.van 't, Lehfeldt, R.A., 1899. Lectures on theoretical and physical chemistry. E. Arnold. https://doi.org/10.5962/bhl.title.17742.
Hollinger, D.Y., Aber, J., Dail, B., Davidson, E.A., Goltz, S.M., Hughes, H., Leclerc, M.Y., Lee, J.T., Richardson, A.D., Rodrigues, C., Scott, N.a., Achuatavarier, D., Walsh, J., 2004. Spatial and temporal variability in forest–atmosphere CO2 exchange. Glob. Chang Biol. 10 (10), 1689–1706. https://doi.org/10.1111/j.1365-2486.2004.00847.x.
Hytteborn, H., Maslov, A., Nazimova, D., Rysin, L., 2005. *Boreal Forests of Eurasia*, pp. 23–99.
Ilvesniemi, H., Levula, J., Ojansuu, R., Kolari, P., Kulmala, L., Pumpanen, J., Launiainen, S., Vesala, T., Nikinmaa, E., 2009. Long-term measurements of the carbon balance of a boreal Scots pine dominated forest ecosystem. Boreal Environ. Res. 14 (4), 731–753. Scopus.
Jõgiste, K., Frelich, L.E., Laarmann, D., Vodde, F., Baders, E., Donis, J., Jansons, A., Kangur, A., Korjus, H., Köster, K., Kusmin, J., Kuuluvainen, T., Marozas, V., Metslaid, M., Metslaid, S., Polyachenko, O., Poska, A., Rebane, S., Stanturf, J.A., 2018. Imprints of management history on hemiboreal forest ecosystems in the Baltic States. Ecosphere 9 (11), e02503. https://doi.org/10.1002/ecs2.2503.
Jactel, H., Petit, J., Desprez-Loustau, M.-L., Delzon, S., Piou, D., Battisti, A., Koricheva, J., 2012. Drought effects on damage by forest insects and pathogens: a meta-analysis. Glob. Chang Biol. 18 (1), 267–276. https://doi.org/10.1111/j.1365-2486.2011.02512.x.
Kannenberg, S.A., Schwalm, C.R., Anderegg, W.R.L., 2020. Ghosts of the past: how drought legacy effects shape forest functioning and carbon cycling. Ecol. Lett. 23 (5), 891–901. https://doi.org/10.1111/ele.13485.
Kljun, N., Calanca, P., Rotach, M.W., Schmid, H.P., 2015. A simple two-dimensional parameterisation for flux footprint prediction (FFP). Geoscientific Model Develop. 8 (11), 3695–3713. https://doi.org/10.5194/gmd-8-3695-2015.
Krasnova, A., Kukumägi, M., Mander, Ü., Torga, R., Krasnov, D., Noe, S.M., Ostonen, I., Püttsepp, Ü., Killian, H., Uri, V., Lõhmus, K., Sõber, J., Soosaar, K., 2019. Carbon exchange in a hemiboreal mixed forest in relation to tree species composition. Agric. For. Meteorol. 275, 11–23. 10.1016/j.agrformet.2019.05.007.
Krasnova, A., Mander, Ü., Noe, S.M., Uri, V., Krasnov, D., Soosaar, K., 2022. Hemiboreal forests' CO2 fluxes response to the European 2018 heatwave. Agric. For. Meteorol. 323, 109042. https://doi.org/10.1016/j.agrformet.2022.109042.
Krishnan, P., Black, T. A., Barr, A. G., Grant, N. J., Gaumont-Guay, D., & Nesic, Z. (2008). Factors controlling the interannual variability in the carbon balance of a southern boreal black spruce forest. J. Geophys. Res.: Atmos., *113*(D9). 10.1029/2007JD008965.
Krishnan, P., Black, T.A., Jassal, R.S., Chen, B., Nesic, Z., 2009. Interannual variability of the carbon balance of three different-aged Douglas-fir stands in the Pacific Northwest. J. Geophysic. Research: Biogeosciences 114 (G4). https://doi.org/10.1029/2008JG000912.
Kuhn, M., 2008. Building predictive models in R using the caret package. J Stat Softw 28, 1–26. https://doi.org/10.18637/jss.v028.i05.
Kurz, W. A., & Apps, M. J. (1999). A 70-Year Retrospective Analysis of Carbon Fluxes in the Canadian Forest Sector. *Ecological Applications, 9*(2), 526–547. 10.1890/1051-0761(1999)009%255B0526:AYRAOC%255D2.0.CO;2.
Kurz, W.A., Stinson, G., Rampley, G.J., Dymond, C.C., Neilson, E.T., 2008. Risk of natural disturbances makes future contribution of Canada's forests to the global carbon cycle highly uncertain. Proc. Natl. Acad. Sci. U. S. A. 105 (5), 1551–1555. 10.1073/pnas.0708133105.
López-Blanco, E., Lund, M., Williams, M., Tamstorf, M.P., Westergaard-Nielsen, A., Exbrayat, J.-F., Hansen, B.U., Christensen, T.R., 2017. Exchange of CO_2 in Arctic tundra: impacts of meteorological variations and biological disturbance. Biogeosciences 14 (19), 4467–4483. https://doi.org/10.5194/bg-14-4467-2017.
Lõhmus, E. (1984). *Eesti metsakasvukohatüübid*. Eesti NSV Agrotööstuskoondise Info- ja Juurutusvalitsus.
Launiainen, S., Katul, G.G., Leppä, K., Kolari, P., Aslan, T., Grönholm, T., Korhonen, L., Mammarella, I., Vesala, T., 2022. Does growing atmospheric CO2 explain increasing carbon sink in a boreal coniferous forest? Glob. chang. Biol. 28 (9), 2910–2929. 10.1111/gcb.16117.
Leisch, F., & Dimitriadou, E. (2021). *mlbench: machine learning benchmark problems* [Manual].
Leverett, R.T., Masino, S.A., Moomaw, W.R., 2021. Older eastern white pine trees and stands accumulate carbon for many decades and maximize cumulative carbon. Frontier. Forest. Glob. Change. 4. https://doi.org/10.3389/ffgc.2021.620450.
Lindroth, A., Lagergren, F., Grelle, A., Klemedtsson, L., Langvall, O., Weslien, P., Tuulik, J., 2009. Storms can cause Europe-wide reduction in forest carbon sink. Glob. chang. Biol. 15 (2), 346–355. 10.1111/j.1365-2486.2008.01719.x.
Lindroth, A., Holst, J., Linderson, M.-L., Aurela, M., Biermann, T., Heliasz, M., Chi, J., Ibrom, A., Kolari, P., Klemedtsson, L., Krasnova, A., Laurila, T., Lehner, I., Lohila, A., Mammarella, I., Mölder, M., Löfvenius, M.O., Peichl, M., Pilegaard, K., Nilsson, M., 2020. Effects of drought and meteorological forcing on carbon and water fluxes in

Nordic forests during the dry summer of 2018. Philosophic. Transac. Royal Soc. B. 375 (1810), 20190516. https://doi.org/10.1098/rstb.2019.0516.
Litton, C.M., Raich, J.W., Ryan, M.G., 2007. Carbon allocation in forest ecosystems. Glob. Chang Biol. 13 (10), 2089–2109. https://doi.org/10.1111/j.1365-2486.2007.01420.x.
Luyssaert, S., Schulze, E.-D., Börner, A., Knohl, A., Hessenmöller, D., Law, B.E., Ciais, P., Grace, J., 2008. Old-growth forests as global carbon sinks. Nature 455 (7210), 213–215. https://doi.org/10.1038/nature07276.
Mamkin, V., Varlagin, A., Yaseneva, I., Kurbatova, J., 2022. Response of spruce forest ecosystem CO2 fluxes to inter-annual climate anomalies in the Southern Taiga. Forests 13 (7). https://doi.org/10.3390/f13071019. Article 7.
Matkala, L., Kulmala, L., Kolari, P., Aurela, M., Bäck, J., 2021. Resilience of subarctic Scots pine and Norway spruce forests to extreme weather events. Agric. For. Meteorol. 296, 108239. 10.1016/j.agrformet.2020.108239.
Mauder, M., Cuntz, M., Drüe, C., Graf, A., Rebmann, C., Schmid, H.P., Schmidt, M., Steinbrecher, R., 2013. A strategy for quality and uncertainty assessment of long-term eddy-covariance measurements. Agric. For. Meteorol. 169, 122–135. https://doi.org/10.1016/j.agrformet.2012.09.006.
Mkhabela, M.S., Amiro, B.D., Barr, A.G., Black, T.A., Hawthorne, I., Kidston, J., McCaughey, J.H., Orchansky, A.L., Nesic, Z., Sass, A., Shashkov, A., Zha, T., 2009. Comparison of carbon dynamics and water use efficiency following fire and harvesting in Canadian boreal forests. Agric. For. Meteorol. 149 (5), 783–794. 10.1016/j.agrformet.2008.10.025.
Moncrieff, J., Massheder, J.M., de Bruin, H., Elbers, J., Friborg, T., Heusinkveld, B., Kabat, P., Scott, S., Soegaard, H., Verhoef, A., 1997. A system to measure surface fluxes of momentum, sensible heat, water vapour and carbon dioxide. J. Hydrol. 188–189, 589–611. https://doi.org/10.1016/S0022-1694(96)03194-0.
Moncrieff, J., Clement, R., Finnigan, J., Meyers, T., 2005. Averaging, detrending, and filtering of Eddy Covariance Time Series. In: Lee, X., Massman, W., Law, B. (Eds.), Handbook of Micrometeorology: A Guide For Surface Flux Measurement and Analysis. Springer, Netherlands, pp. 7–31. https://doi.org/10.1007/1-4020-2265-4_2.
Papale, D., Reichstein, M., Aubinet, M., Canfora, E., Bernhofer, C., Kutsch, W., Longdoz, B., Rambal, S., Valentini, R., Vesala, T., Yakir, D., 2006. Towards a standardized processing of Net Ecosystem Exchange measured with eddy covariance technique: algorithms and uncertainty estimation. Biogeosciences 3 (4), 571–583. https://doi.org/10.5194/bg-3-571-2006.
Peichl, M., Martínez-García, E., Fransson, J.E.S., Wallerman, J., Laudon, H., Lundmark, T., Nilsson, M.B., 2023. Landscape-variability of the carbon balance across managed boreal forests. Glob. Chang Biol. 29 (4), 1119–1132. https://doi.org/10.1111/gcb.16534.
Perkins, S.E., Alexander, L.V., 2013. On the Measurement of Heat Waves. J. clim. 26 (13), 4500–4517. 10.1175/JCLI-D-12-00383.1.
Perkins, S.E., Lewis, S.C., 2020. Increasing trends in regional heatwaves. Nature Communications 11 (1), 3357. 10.1038/s41467-020-16970-7.
Piao, S., Ciais, P., Friedlingstein, P., Peylin, P., Reichstein, M., Luyssaert, S., Margolis, H., Fang, J., Barr, A., Chen, A., Grelle, A., Hollinger, D.Y., Laurila, T., Lindroth, A., Richardson, A.D., Vesala, T., 2008. Net carbon dioxide losses of northern ecosystems in response to autumn warming. Nature 451 (7174), 49–52. https://doi.org/10.1038/nature06444.
Potapov, P., Yaroshenko, A., Turubanova, S., Dubinin, M., Laestadius, L., Thies, C., Aksenov, D., Egorov, A., Yesipova, Y., Glushkov, I., Karpachevskiy, M., Kostikova, A., Manisha, A., Tsybikova, E., Zhuravleva, I., 2008. Mapping the World's Intact Forest Landscapes by Remote Sensing. Ecol. Soc. 13 (2), 51. 10.5751/es-02670-130251.
Pretzsch, H., Schütze, G., Uhl, E., 2013. Resistance of European tree species to drought stress in mixed versus pure forests: Evidence of stress release by inter-specific facilitation. Plant Biology 15 (3), 483–495. 10.1111/j.1438-8677.2012.00670.x.
Qu, L.-P., Chen, J., Xiao, J., De Boeck, H.J., Dong, G., Jiang, S.-C., Hu, Y.-L., Wang, Y.-X., Shao, C.-L., 2024. The complexity of heatwaves impact on terrestrial ecosystem carbon fluxes: factors, mechanisms and a multi-stage analytical approach. Environ. Res. 240, 117495. https://doi.org/10.1016/j.envres.2023.117495.
R Core Team, 2021. *R: a Language and Environment For Statistical Computing* [Manual]. R Foundation for Statistical Computing. https://www.R-project.org/.
Reichstein, M., Kätterer, T., Andrén, O., Ciais, P., Schulze, E.-D., Cramer, W., Papale, D., Valentini, R., 2005a. Temperature sensitivity of decomposition in relation to soil organic matter pools: critique and outlook. Biogeosciences 2 (4), 317–321. https://doi.org/10.5194/bg-2-317-2005.
Reichstein, M., Subke, J.-A., Angeli, A.C., Tenhunen, J.D., 2005b. Does the temperature sensitivity of decomposition of soil organic matter depend upon water content, soil horizon, or incubation time? Glob. Chang. Biol. 11 (10), 1754–1767. https://doi.org/10.1111/j.1365-2486.2005.001010.x.
Schuldt, B., Buras, A., Arend, M., Vitasse, Y., Beierkuhnlein, C., Damm, A., Gharun, M., Grams, T.E.E., Hauck, M., Hajek, P., Hartmann, H., Hiltbrunner, E., Hoch, G., Holloway-Phillips, M., Körner, C., Larysch, E., Lübbe, T., Nelson, D.B., Rammig, A., Kahmen, A., 2020. A first assessment of the impact of the extreme 2018 summer drought on Central European forests. Basic Appl. Ecol. 45, 86–103. https://doi.org/10.1016/j.baae.2020.04.003.
Shahbaz, M., Bengtson, P., Mertes, J.R., Kulessa, B., Kljun, N., 2022. Spatial heterogeneity of soil carbon exchanges and their drivers in a boreal forest. Sci. Total Environ. 831, 154876. https://doi.org/10.1016/j.scitotenv.2022.154876.
Smith, N.E., Kooijmans, L.M.J., Koren, G., van Schaik, E., van der Woude, A.M., Wanders, N., Ramonet, M., Xueref-Remy, I., Siebicke, L., Manca, G., Brümmer, C., Baker, I.T., Haynes, K.D., Luijkx, I.T., Peters, W., 2020. Spring enhancement and summer reduction in carbon uptake during the 2018 drought in northwestern Europe. Philosophic. Transaction. Royal Soc. B. 375 (1810), 20190509. https://doi.org/10.1098/rstb.2019.0509.
Stephens, J.J., Black, T.A., Jassal, R.S., Nesic, Z., Grant, N.J., Barr, A.G., Helgason, W.D., Richardson, A.D., Johnson, M.S., Christen, A., 2018. Effects of forest tent caterpillar defoliation on carbon and water fluxes in a boreal aspen stand. Agri. Forest Meteorol. 253–254, 176–189. https://doi.org/10.1016/j.agrformet.2018.01.035.
Stokland, J.N., 2021. Volume increment and carbon dynamics in boreal forest when extending the rotation length towards biologically old stands. For. Ecol. Manage. 488, 119017. https://doi.org/10.1016/j.foreco.2021.119017.
Suni, T., Berninger, F., Markkanen, T., Keronen, P., Rannik, Ü., & Vesala, T. (2003). Interannual variability and timing of growing-season CO2 exchange in a boreal forest. J. Geophy. Res.: Atmos. 108(D9). 10.1029/2002JD002381.
Tremblay, S.L., D'Orangeville, L., Lambert, M.-C., Houle, D., 2018. Transplanting boreal soils to a warmer region increases soil heterotrophic respiration as well as its temperature sensitivity. Soil Biol. Biochem. 116, 203–212. https://doi.org/10.1016/j.soilbio.2017.10.018.
Ueyama, M., Iwata, H., Harazono, Y., 2014. Autumn warming reduces the CO2 sink of a black spruce forest in interior Alaska based on a nine-year eddy covariance measurement. Glob Chang Biol 20 (4), 1161–1173. https://doi.org/10.1111/gcb.12434.
Uri, V., Kukumägi, M., Aosaar, J., Varik, M., Becker, H., Aun, K., Krasnova, A., Morozov, G., Ostonen, I., Mander, Ü., Lõhmus, K., Rosenvald, K., Kriiska, K., Soosaar, K., 2019. The carbon balance of a six-year-old Scots pine (*Pinus sylvestris* L.) ecosystem estimated by different methods. For. Ecol. Manage. 433, 248–262. https://doi.org/10.1016/j.foreco.2018.11.012.
Uri, V., Kukumägi, M., Aosaar, J., Varik, M., Becker, H., Aun, K., Nikopensius, M., Uri, M., Buht, M., Sepaste, A., Padari, A., Asi, E., Sims, A., Karoles, K., 2022. Litterfall dynamics in Scots pine (*Pinus sylvestris*), Norway spruce (*Picea abies*) and birch (*Betula*) stands in Estonia. For. Ecol. Manage. 520, 120417. https://doi.org/10.1016/j.foreco.2022.120417.
Vesala, T., Launiainen, S., Kolari, P., Pumpanen, J., Sevanto, S., Hari, P., Nikinmaa, E., Kaski, P., Mannila, H., Ukkonen, E., Piao, S.L., Ciais, P., 2010. Autumn temperature and carbon balance of a boreal Scots pine forest in Southern Finland. Biogeosciences 7 (1), 163–176. https://doi.org/10.5194/bg-7-163-2010.
von Buttlar, J., Zscheischler, J., Rammig, A., Sippel, S., Reichstein, M., Knohl, A., Jung, M., Menzer, O., Arain, M.A., Buchmann, N., Cescatti, A., Gianelle, D., Kiely, G., Law, B.E., Magliulo, V., Margolis, H., McCaughey, H., Merbold, L., Migliavacca, M., Mahecha, M.D., 2018. Impacts of droughts and extreme-temperature events on gross primary production and ecosystem respiration: a systematic assessment across ecosystems and climate zones. Biogeosciences 15 (5), 1293–1318. https://doi.org/10.5194/bg-15-1293-2018.
Wang, X., Liu, L., Piao, S., Janssens, I.A., Tang, J., Liu, W., Chi, Y., Wang, J., Xu, S., 2014. Soil respiration under climate warming: differential response of heterotrophic and autotrophic respiration. Glob. Chang. Biol. 20 (10), 3229–3237. https://doi.org/10.1111/gcb.12620.
Welp, L.R., Randerson, J.T., Liu, H.P., 2007. The sensitivity of carbon fluxes to spring warming and summer drought depends on plant functional type in boreal forest ecosystems. Agric For Meteorol 147 (3), 172–185. https://doi.org/10.1016/j.agrformet.2007.07.010.
Wutzler, T., Lucas-Moffat, A., Migliavacca, M., Knauer, J., Sickel, K., Šigut, L., Menzer, O., Reichstein, M., 2018. Basic and extensible post-processing of eddy covariance flux data with REddyProc. Biogeosciences 15 (16), 5015–5030. https://doi.org/10.5194/bg-15-5015-2018.
Xia, J., Niu, S., Ciais, P., Janssens, I.A., Chen, J., Ammann, C., Arain, A., Blanken, P.D., Cescatti, A., Bonal, D., Buchmann, N., Curtis, P.S., Chen, S., Dong, J., Flanagan, L.B., Frankenberg, C., Georgiadis, T., Gough, C.M., Hui, D., Luo, Y., 2015. Joint control of terrestrial gross primary productivity by plant phenology and physiology. Proceed. Nation. Acad. Science. 112 (9), 2788–2793. https://doi.org/10.1073/pnas.1413090112.
Xu, H., Xiao, J., Zhang, Z., 2020. Heatwave effects on gross primary production of northern mid-latitude ecosystems. Environment. Res. Lett. 15 (7), 074027. https://doi.org/10.1088/1748-9326/ab8760.
Yan, Y., Zhou, L., Zhou, G., Wang, Y., Song, J., Zhang, S., Zhou, M., 2023. Extreme temperature events reduced carbon uptake of a boreal forest ecosystem in Northeast China: evidence from an 11-year eddy covariance observation. Front. Plant Sci. 14. https://www.frontiersin.org/articles/10.3389/fpls.2023.1119670.
Yu, L., Wang, Y., Wang, Y., Sun, S., Liu, L., 2015. Quantifying components of soil respiration and their response to abiotic factors in two typical subtropical forest stands, Southwest China. Plos One 10 (2), e0117490. https://doi.org/10.1371/journal.pone.0117490.
Yvon-Durocher, G., Jones, J.I., Trimmer, M., Woodward, G., Montoya, J.M., 2010. Warming alters the metabolic balance of ecosystems. Philosophic. Transac. Royal Soc. B. 365 (1549), 2117–2126. https://doi.org/10.1098/rstb.2010.0038.
Zhang, H., Wu, P., Yin, A., Yang, X., Zhang, M., Gao, C., 2017. Prediction of soil organic carbon in an intensively managed reclamation zone of eastern China: a comparison of multiple linear regressions and the random forest model. Sci. Total Environ. 592, 704–713. https://doi.org/10.1016/j.scitotenv.2017.02.146.
Zhang, M., Sayer, E.J., Zhang, W., Ye, J., Yuan, Z., Lin, F., Hao, Z., Fang, S., Mao, Z., Ren, J., Wang, X., 2022. Seasonal influence of biodiversity on soil respiration in a temperate forest. Plant. 11 (23), 3391. https://doi.org/10.3390/plants11233391.